

2. EXPLANATORY NOTES¹

Shipboard Scientific Party²

INTRODUCTION

In this chapter, we have assembled information that will help the reader understand the basis for our preliminary conclusions and also help the interested investigator select samples for further analysis. This information concerns only shipboard operations and analyses described in the site reports in the *Initial Results* volume of the Leg 146 *Proceedings of the Ocean Drilling Program*. Methods used by various investigators for shore-based analysis of Leg 146 data will be detailed in the individual scientific contributions published in the *Scientific Results* volume.

Authorship of Site Chapters

The separate sections of the site chapters were written by the following shipboard scientists (authors are listed in alphabetical order, no seniority is necessarily implied):

Site Summary: Carson, Westbrook
Background and Objectives: Carson, Westbrook
Seismic Stratigraphy: Moore, Westbrook
Operations: Foss, Musgrave
Lithostratigraphy: Baranov, Camerlenghi, Chamov, Clennell, Dietrich, Kopf, Tobin
Biostratigraphy: Caulet, Zellers
Paleomagnetism: Housen, Musgrave, Sato
Structural Geology: Baranov, Housen, Tobin
Organic Geochemistry: Hovland, Whiticar
Gas Hydrate Studies: Foucher, Hovland, Kastner, Sample, Whiticar
Inorganic Geochemistry: Kastner, Sample, Whiticar
Physical Properties: Ashi, Brown, Foucher, Moran
WSTP and ADARA Temperature Measurements: Brown, Foucher
Lateral Stress Tool (LAST): Moran
Packer Experiments: Sreaton
Logging: Jarrard, MacKay, Moore, Sreaton
Summary and Conclusions: Carson, Westbrook

Following the text of each site chapter are summary core descriptions ("barrel sheets"), photographs of each core, and tables of smear slide observations.

Geophysical Survey Data

Data collected during site surveys before Leg 146 are presented in the "Seismic Stratigraphy" section of the individual site chapters. During Leg 146 *JOIDES Resolution* transits 3.5- and 12-kHz echosounder and magnetic data were recorded.

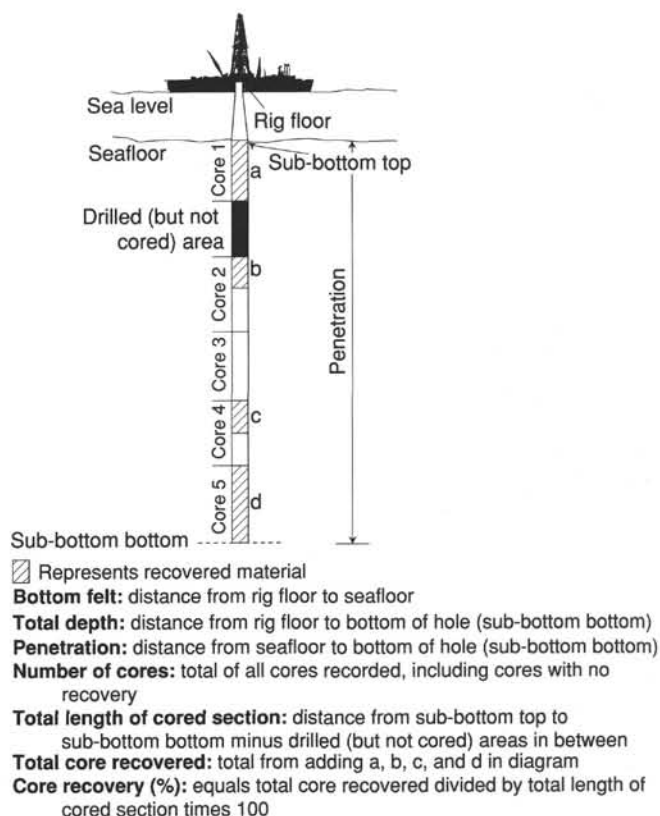
Bathymetric data collected using the 3.5- and 12-kHz precision depth recorder (PDR) system were displayed on two Raytheon recorders. The depths were calculated on the basis of an assumed 1463 m/s sound velocity in water. The water depth (in meters) at each site was corrected for (1) the variation in sound velocity with depth using

Matthews's (1939) tables and (2) the depth of the transducer pod (6.8 m) below sea level. In addition, depths referred to the drilling-platform level are corrected for the height of the rig floor above the water line, which gradually increased from 10.7 to 11.0 m throughout the cruise (see Fig. 1).

Magnetic data were collected using a Geometrics 801 proton precession magnetometer, displayed on a strip chart recorder, and recorded on magnetic tape for later processing.

Drilling Characteristics

Because water circulation downhole is open, cuttings are lost onto the seafloor and cannot be examined. Information concerning sedimentary stratification in uncored or unrecovered intervals may be inferred from seismic data, wireline-logging results, and an examination of the behavior of the drill string as observed and recorded on the drilling platform. Typically, the harder a layer, the slower and more difficult it is to penetrate. A number of other factors may determine the rate of penetration, so it is not always possible to relate the drilling time directly to the hardness of the layers. Bit weight and revolutions per minute, recorded on the drilling recorder, also influence the penetration rate.



¹ Westbrook, G.K., Carson, B., Musgrave, R.J., et al., 1994. *Proc. ODP, Init. Repts.*, 146 (Pt. 1): College Station, TX (Ocean Drilling Program).

² Shipboard Scientific Party is as given in the list of participants preceding the contents.

Figure 1. Diagram illustrating terms used in the discussion of coring operations and core recovery.

When cores are split, many show signs of significant sediment disturbance, including the concave-downward appearance of originally horizontal bands, haphazard mixing of lumps of different lithologies (mainly at the tops of cores), and the near-fluid state of some sediments recovered from tens to hundreds of meters below the seafloor. Core deformation probably occurs during cutting, retrieval (with accompanying changes in pressure and temperature), and core handling on deck, and overprints natural deformation structures.

Shipboard Scientific Procedures

Numbering of Sites, Holes, Cores, and Samples

Drilling sites are numbered consecutively from the first Deep Sea Drilling Project (DSDP) site drilled by the *Glomar Challenger* in 1968. A site number refers to one or more holes drilled while the ship was positioned over one acoustic beacon. Multiple holes may be drilled at a single site by pulling the drill pipe above the seafloor (out of the hole), moving the ship some distance from the previous hole, and then drilling another hole. In some cases, the ship may return to a previously occupied site to drill additional holes.

For all ODP drill sites, a letter suffix distinguishes each hole drilled at the same site. For example, the first hole drilled is assigned the site number modified by the suffix *A*, the second hole takes the site number and suffix *B*, and so forth. Note that this procedure differs slightly from that used by DSDP (Sites 1 through 624), but prevents ambiguity between site- and hole-number designations. It is important to distinguish among holes drilled at a site, because recovered sediments or rocks from the same depth in different holes do not necessarily represent equivalent positions in the stratigraphic column.

The cored interval is measured in meters below seafloor (mbsf); sub-bottom depths are determined by subtracting the drill-pipe measurement (DPM) water depth (the length of pipe from the rig floor to the seafloor) from the total DPM (from the rig floor to the bottom of the hole; see Fig. 1). Note that although the echo-sounding data (from the precision depth recorders) are used to locate the site, they are not used as a basis for any further measurements.

The depth interval assigned to an individual core begins with the depth below the seafloor that the coring operation began and extends to the depth that the coring operation ended for that core (see Fig. 1). For rotary coring using the rotary core barrel or extended core barrel (RCB and XCB, respectively), each coring interval is equal to the length of the joint of drill pipe added for that interval (though a shorter core may be attempted in special instances). The drill pipe in use varies from about 9.4 to 9.8 m. The pipe is measured as it is added to the drill string, and the cored interval is recorded as the length of the pipe joint to the nearest 0.1 m. For advanced hydraulic piston coring (APC) operations, the drill string is advanced 9.5 m, the maximum length of the piston stroke.

Coring intervals may be shorter and may not necessarily be adjacent if separated by drilled intervals. In soft sediments, the drill string can be "washed ahead" with the core barrel in place, without recovering sediments. This is achieved by pumping water down the pipe at high pressure to wash the sediment out of the way of the bit and up the annulus between the drill pipe and the wall of the hole. If thin, hard, rock layers are present, then it is possible to get "spotty" sampling of these resistant layers within the washed interval, and thus to have a cored interval greater than 9.5 m. In drilling hard rock, a center bit may replace the core barrel if it is necessary to drill without core recovery.

Cores taken from a hole are numbered serially from the top of the hole downward. Core numbers and their associated cored intervals in meters below seafloor usually are unique in a given hole; however, this may not be true if an interval must be cored twice, because of caving of cuttings or other hole problems. Maximum full recovery for a single core is 9.5 m of rock or sediment contained in a plastic liner (6.6-cm internal diameter) plus about 0.2 m (without a plastic liner) in the core catcher (Fig. 2). The core catcher is a device at the bottom

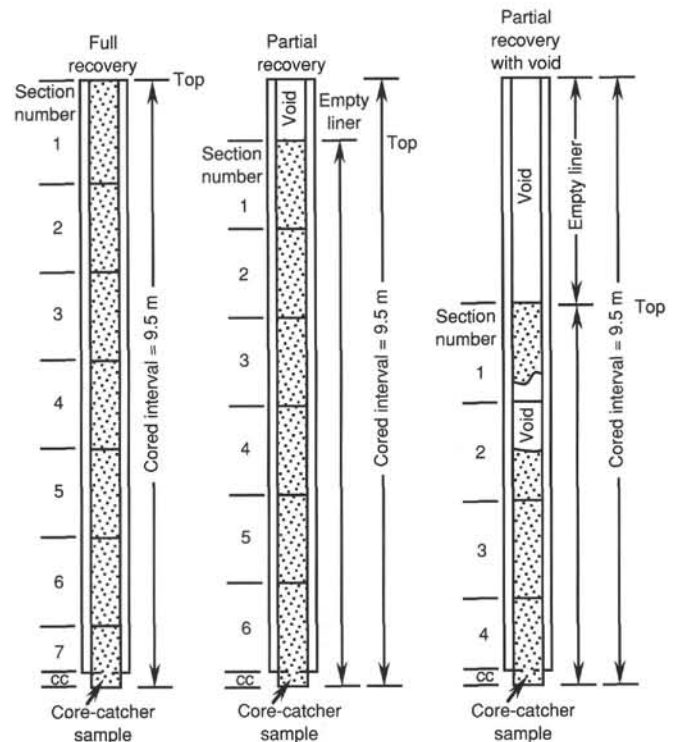


Figure 2. Diagram showing procedure used in cutting and labeling core sections.

of the core barrel which prevents the core from sliding out when the barrel is being retrieved from the hole. For sediments, the core-catcher sample is extruded into a short piece of plastic liner and is treated as a separate section below the last core section. For hard rocks, the material recovered in the core catcher is included at the bottom of the last section. In certain situations (e.g., when coring gas-charged sediments that expand while being brought on deck) recovery may exceed the 9.5-m maximum.

A recovered sedimentary core is divided into 1.5-m sections that are numbered serially from the top (Fig. 2). When full recovery is obtained, the sections are numbered from 1 through 7, with the last section possibly being shorter than 1.5 m (rarely, an unusually long core may require more than seven sections). When less than full recovery is obtained, there will be as many sections as needed to accommodate the length of the core recovered; for example, 4 m of core would be divided into two 1.5-m sections and one 1-m section. If cores are fragmented (recovery less than 100%), sections are numbered serially and intervening sections are noted as void, whether shipboard scientists think that the fragments were contiguous in situ or not. In rare cases a section less than 1.5 m may be cut in order to preserve features of interest (e.g., lithologic contacts).

By convention, during the core description material recovered from the core catcher of a sedimentary core is placed in a separate section labeled core catcher (CC) below the last section recovered in the liner. The core catcher is placed at the top of the cored interval in cases where material is recovered only in the core catcher. However, information supplied by the drillers or by other sources may allow for more precise interpretation as to the correct position of core-catcher material within an incompletely recovered cored interval.

When, as is usually the case, the recovered core is shorter than the cored interval, the top of the core is equated with the top of the cored interval by convention, in order to achieve consistency in handling analytical data derived from the cores. Samples removed from the cores are designated by the distance measured in centimeters from the top of the section to the top and bottom of each sample removed from

that section. In curated hard-rock sections, sturdy plastic spacers are placed between pieces that did not fit together in order to protect them from damage in transit and in storage; therefore, the centimeter interval noted for a hard-rock sample has no direct relationship to that sample's depth within the cored interval, but is only a physical reference to the location of the sample within the curated core.

A full identification number for a sample consists of the following information: leg, site, hole, core number, core type, section number, piece number (for hard rock), and interval in centimeters measured from the top of section. For example, a sample identification of "146-888B-5H-1, 10–12 cm" would be interpreted as representing a sample removed from the interval between 10 and 12 cm below the top of Section 1, Core 5 (H designates that this core was taken during hydraulic piston coring) of Hole 888B during Leg 146.

All ODP core identifiers indicate core type. The following abbreviations are used: R = rotary core barrel; H = hydraulic piston core (HPC; also referred to as APC); N = motor-driven core barrel (MDCB, or "Navidrill"); P = pressure core sampler (PCS); V = vibra-percussive corer (VPC); X = extended core barrel; B = drill-bit recovery; C = center-bit recovery; W = wash-core recovery; and M = miscellaneous material. APC, XCB, RCB, MDCB, PCS, VPC, and wash cores were cut on Leg 146.

Core Handling

Sediments

As soon as a core is retrieved on deck, a sample is taken from the core catcher and given to the paleontological laboratory for an initial age assessment. The core is then placed on the long horizontal rack, and gas samples may be taken by piercing the core liner and withdrawing gas into a vacuum-tube ("vacutainer" method). Voids within the core are sought as sites for gas sampling. Next, the core is marked into section lengths, each section is labeled, and the core is cut into sections. Interstitial-water (IW) whole-round samples are then taken as a matter of ODP policy; whole-round samples for organic geochemistry may also be taken at this stage if they have been requested. Because of the short survival time of gas hydrates when recovered and exposed to surface temperatures and pressures, gas hydrate samples are immediately removed from the core and placed either in pressure vessels or in liquid nitrogen. In some cases gas hydrate sampling requires the removal of whole-round samples. In addition, some headspace gas samples are removed by insertion of a cylindrical syringe into the ends of cut sections on the catwalk, and sealed in glass vials for light hydrocarbon analysis. Some microbiology and physical properties samples were also taken as small cylinders from cut ends of sections. Each section is then sealed at the top and bottom by gluing on color-coded plastic caps, blue to identify the top of a section and clear for the bottom. A yellow cap is placed on the section ends from which a whole-round sample has been removed, and the sample code (e.g., IW) is written on the yellow cap. The caps are usually attached to the liner by coating the end of the liner and the inside rim of the cap with acetone, and then the caps are taped to the liners.

The cores then are carried into the laboratory, where the sections are again labeled, using an engraver to permanently mark the full designation of the section. The length of the core in each section and the core-catcher sample are measured to the nearest centimeter; this information is logged into the shipboard CORELOG database program.

Sections from APC and XCB cores are normally run through the multisensor track (MST) before splitting. The MST includes the gamma-ray attenuation porosity evaluator (GRAPE) and *P*-wave logger devices, which measure bulk density, porosity, and sonic velocity, and also includes a meter that determines the volume magnetic susceptibility. At this point, whole-round samples for physical properties (PP) and structural analysis are taken. In well-lithified sedimentary cores, the core liner is split and the top half removed so that the whole-round core can be observed before choosing the samples. Relatively soft sedimentary cores are equilibrated to room tem-

perature (approximately 3 hr) and thermal conductivity measurements are performed on them before being split.

Cores of soft material are split lengthwise into working and archive halves. The softer cores are split with a wire or saw, depending on the degree of induration. Harder cores are split with a band saw or diamond saw. The wire-cut cores are split from the bottom to top, so investigators should be aware that older material could have been transported up the core on the split face of each section.

The working half of the core is sampled for both shipboard and shore-based laboratory studies. Each extracted sample is logged into the sampling computer database program by its location and the name of the investigator receiving the sample. Records of all removed samples are kept by the curator at ODP. The extracted samples are sealed in plastic vials or bags and labeled. Samples are routinely taken for shipboard physical property analysis. These samples are subsequently used to determine calcium carbonate (coulometric analysis) and organic carbon (NCS elemental analyzer); the data are reported in the site chapters.

The archive half is described visually. Smear slides made from samples taken from the archive half are supplemented by thin sections taken from the working half. Most archive sections are run through the cryogenic magnetometer. The archive half is then photographed with both black-and-white and color film, a whole core at a time. Close-up photographs (black-and-white) are taken of particular features, as requested by individual scientists.

Both halves of the core are then put into labeled plastic tubes, sealed, and transferred to cold-storage space aboard the drilling vessel. At the end of the leg, the cores are transferred from the ship in refrigerated air-freight containers to cold storage at the Gulf Coast Repository at the Ocean Drilling Program, Texas A&M University, College Station, Texas.

Fluids

In addition to the routine recovery of gas and liquid samples from sediment cores brought on deck, techniques have been developed for the recovery of fluids at conditions near to those applying in situ down the drill hole. The PCS maintains downhole hydrostatic pressures up to approximately 70 MPa (10,000 lb/in.²) while recovering a core sample with a nominal diameter of 42 mm and a length of 0.86 m. Although direct sampling of the pressured core is not yet possible, fluid and gas samples can be recovered. The water-sampling temperature probe (WSTP) extracts interstitial water from sediments at the bottom of the hole after being lowered down the drill pipe on the sand line. Its filter probe extends more than 1 m beyond the end of the drill bit.

LITHOSTRATIGRAPHY

Sediment Core Description

"Barrel Sheets" and Visual Core Description Forms

The core description forms (Fig. 3), or barrel sheets, summarize the data obtained during the shipboard analyses of each sediment core. These were generated using the ODP in-house Macintosh application VCD (Edition 1.0.1, §14), customized for use on Leg 146. The following discussion explains the ODP conventions used in compiling each part of the core description forms, the use of VCD to generate these forms, and the exceptions to these procedures adopted by the Leg 146 shipboard party.

Shipboard sedimentologists were responsible for visual core logging, smear slide analyses, and thin-section descriptions of sedimentary and volcanoclastic material. Core descriptions were initially recorded at the section scale by hand on standard ODP visual core description (VCD) forms. Use of these VCD forms is considered optional by ODP, but the Leg 146 scientific party considered it desirable to preserve fine-detail observations that are lost at the core-by-core level of the barrel sheets. Structural geologists also

SITE 888 HOLE A CORE 1H					CORED 0.0 - 9.5 mbsf			
Meter	Graphic Lith.	Section	Age	Structure	Disturb	Sample	Color	Description
1	[Symbol]	1			OO	S		CLAYEY SILT WITH DIATOMS and FINE SAND
2	[Symbol]	2		***	OO	D	5Y 3/2	Major Lithologies: CLAYEY SILT WITH DIATOMS, with biogenic fraction composed of diatoms, sponge spicules, radiolarians, and siliciclastic fraction composed of volcanic glass, heavy minerals, hornblende, and feldspars. Color is dark greenish gray (5Y 3/2) to olive gray (5Y 4/1). The sediment is well sorted.
3	[Symbol]	3		***	OO			FINE SAND: extremely well sorted sand with rounded and sub-angular grains. Components are pyroxene, rock fragments, feldspars, hornblende, and volcanic glass. Color is dark gray (N3).
4	[Symbol]	4		***	OO	S	5Y 4/1 To N3	Minor Lithology: SILTY CLAY WITH PEBBLES: sediment with similar composition to the siliciclastic fraction of the silt with diatoms. It occurs at the bottom of Core 146-888A-1H, in Section 6 (90-150 cm) and Section 7. The color is dark gray (N4). Pebbles are centimeter-size, dark gray, and matrix supported.
5	[Symbol]	5			OO			
6	[Symbol]	6		***	OO	S	N3	General Description: The sedimentary section recovered in Core 146-888A-1H is an alternation of clayey silt and fine sand. The sand beds vary in thickness from a few centimeters to about 100 cm, and often show sharp basal contact and fining upward gradation. The silt is often parallel laminated. Genesis of the sediment: turbiditic.
7	[Symbol]	7			OO			
8	[Symbol]	6		***	OO	S		
9	[Symbol]	7		***	OO	S	5Y 3/2 To N4	
CC	[Symbol]					M		

Figure 3. Core description form ("barrel sheet") used for sediments and sedimentary rocks.

recorded structures on VCD forms of their own design. The VCD forms are available from ODP on request.

For each hole a master chart was prepared (Fig. 4), which indicates recovery, summarizes the lithology, and charts a variety of data against sub-bottom depth (biostratigraphic zones, magnetochrons, structural geology, chemistry, physical properties, paleotemperatures, and paleodepths). The master charts supplement the information contained on the barrel sheets, at a further condensed scale.

Core Designation

Cores are designated using leg, site, hole, core number, and core type as discussed in a preceding section (see "Numbering of Sites, Holes, Cores, and Samples" section, this chapter). The cored interval is specified in terms of meters below sea level (mbsl) and mbsf. On the basis of drill-pipe measurements, reported by the SEDCO coring technician and the ODP operations superintendent, depths are corrected for the height above sea level of the dual elevator stool on the rig floor to give the true water depth and correct depth of datums below sea level.

Graphic Lithology

The lithology of the material recovered is represented on the core description form (barrel sheet) by up to three symbols in the column titled "Graphic Lithology" (Fig. 5). Where an interval of sediment or sedimentary rock is a homogenous mixture, the constituent categories are separated by a solid vertical line, with each category represented by its own symbol. Constituents accounting for <10% of the sediment in a given lithology (or others remaining after the representation of the three most abundant lithologies) are not shown in the "Graphic Lithology" column but are listed in the lithologic "Description" section of the core description form. In an interval comprising two or more sediment lithologies that have quite different compositions, such as in thin-bedded and highly variegated sediments, the average relative abundances of the lithologic constituents are represented graphically by dashed lines that vertically divide the interval into appropriate fractions, as described previously. The "Graphic Lithology" column shows only the composition of individual layers or intervals exceeding 20 cm in thickness.

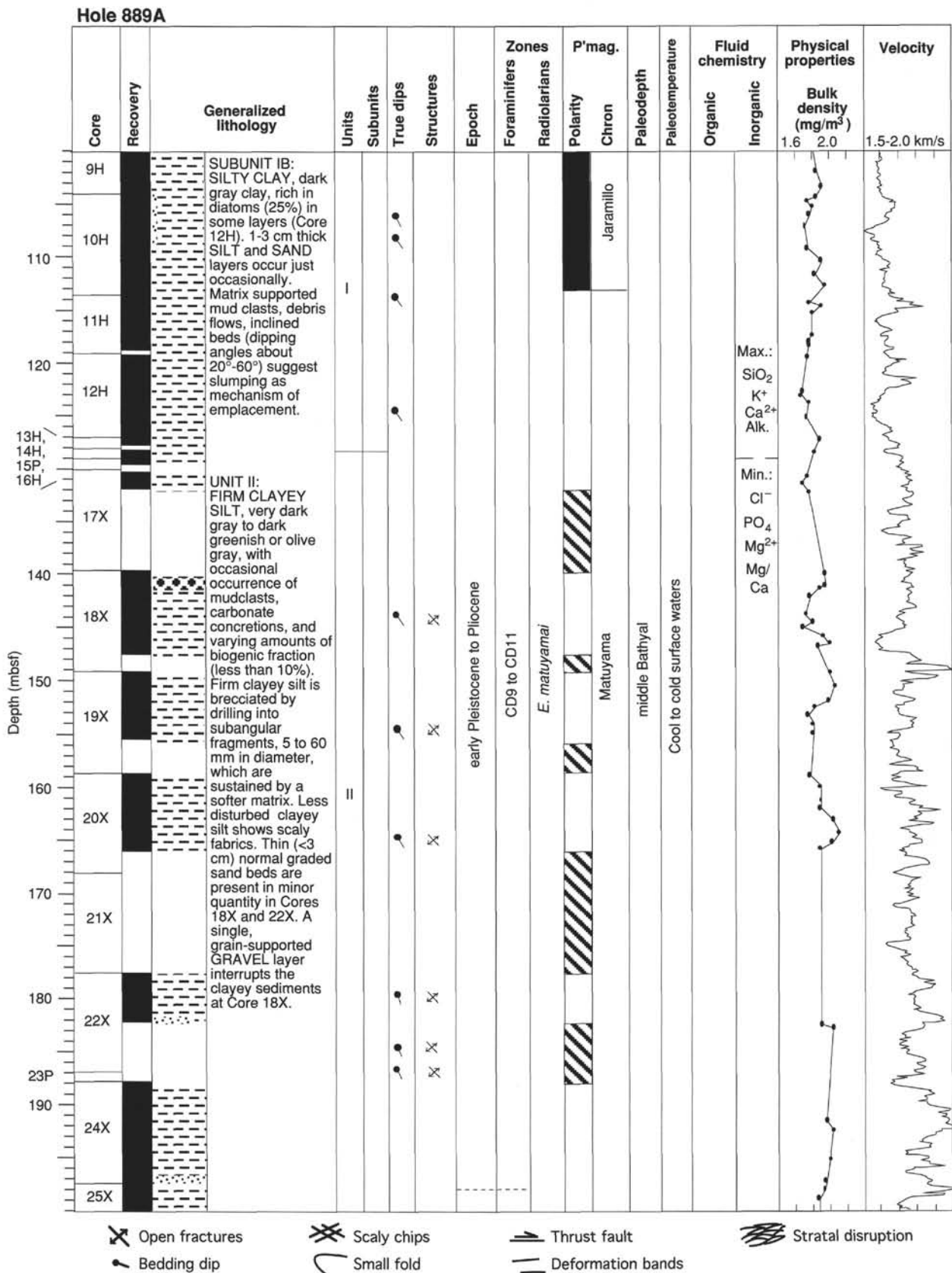


Figure 4. Example of a hole master chart. Lithologic symbols are as for barrel sheets (Fig. 3). Additional symbols used in the "Structures" column are indicated.

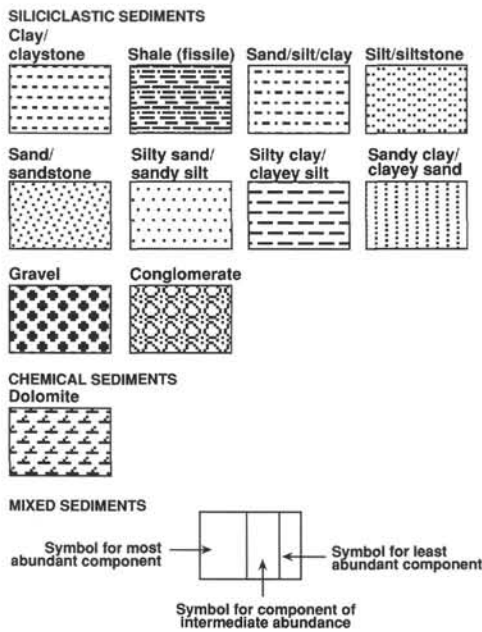


Figure 5. Key to symbols used in the "graphic lithology" column on the core description form shown in Figure 3.

Age

The chronostratigraphic unit, as recognized on the basis of paleontological and paleomagnetic criteria, is shown in the "Age" column on the core description form. Detailed information on the biostratigraphic zonation is presented in the "Biostratigraphy" section in each site report chapter.

Sedimentary Structures

In sediment cores, natural structures and structures created by the coring process can be difficult to distinguish. Natural sedimentary structures observed are indicated by symbols entered in the "Structure" column of the core description form (Fig. 6).

Sediment Disturbance

Sediment disturbance resulting from the coring process is illustrated in the "Disturbance" column on the core description form (using symbols in Fig. 6). Blank regions indicate a lack of drilling disturbance. The degree of drilling disturbance is described for soft and firm sediments using the following categories:

1. Slightly deformed: bedding contacts are slightly bent.
2. Moderately deformed: bedding contacts have undergone extreme bowing.
3. Highly deformed: bedding is completely disturbed and can show symmetrical diapir-like or flow structures.
4. Soupy: intervals are water saturated and have lost all aspects of original bedding.

The degree of fracturing in indurated sediments is described using the following categories:

1. Slightly fractured: core pieces are in place and contain little drilling slurry or breccia.
2. Moderately fragmented: core pieces are in place or partly displaced, but original orientation is preserved or recognizable (drilling slurry may surround fragments).
3. Highly fragmented: pieces are from the interval cored and probably in correct stratigraphic sequence (although they may not represent the entire section), but original orientation is completely lost.

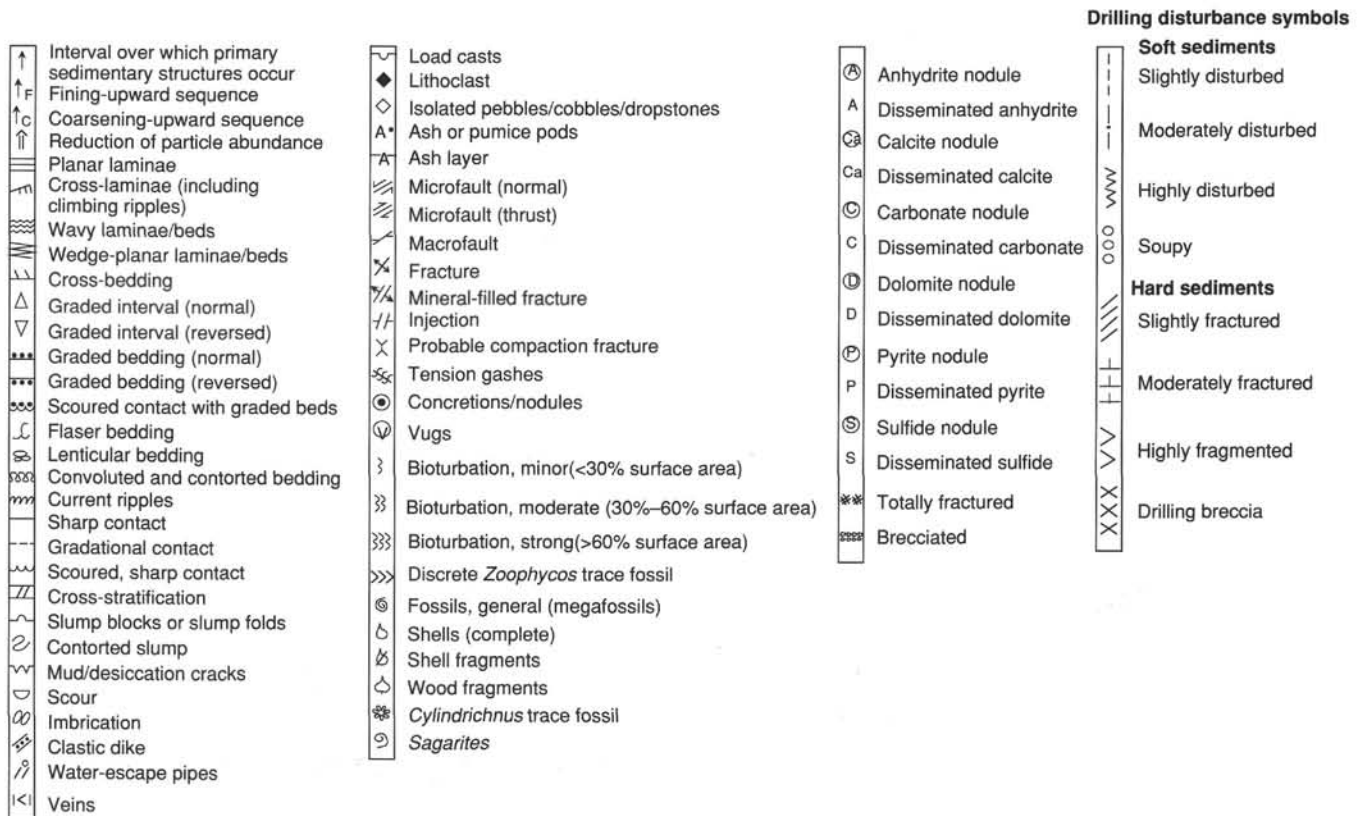


Figure 6. Symbols used for drilling disturbance and sedimentary structure on core description forms shown in Figure 3.

4. Drilling breccia: core pieces have lost their original orientation and stratigraphic position and may be mixed with drilling slurry.

Color

At Site 888, the hue and chroma attributes of color were determined by comparison with Munsell soil-color charts (1971) as soon as possible after the cores were split because redox-associated color changes may occur when deep-sea sediments are exposed to the atmosphere. At Sites 889, 890, 891, and 892, the Minolta color spectrophotometer (Model CM 2002) was used to provide a more accurate determination of color. Information on core colors is given in the "Color" column on the core description form.

Samples

The position of samples taken from each core for shipboard sedimentological analysis and of whole-round samples removed from the core is indicated in the "Samples" column on the core description form (Fig. 3). The symbol "S" indicates the location of smear slide samples, the symbol "T" indicates the location of thin-section samples, and the symbol "M" indicates the location of paleontology samples. The notation "IW" designates the location of whole-round samples for interstitial-water geochemistry, and "W" indicates the location of all other whole-round samples.

Lithologic Description—Text

The lithologic description that appears on each core description form consists of three parts: (1) a heading that lists all the major sediment lithologies (see "Sedimentology" section, this chapter) observed in the core, (2) a heading for minor lithologies (see "Sedimentology" section, this chapter), and (3) a more detailed description of these sediments, including the location in the core of significant features. Descriptions and locations of thin, interbedded, or minor lithologies that cannot be depicted in the "Graphic Lithology" column are included in the text.

Smear Slide Summary

A table summarizing data from smear slides and thin sections appears at the end of each site chapter. The table includes information on the sample location, whether the sample represents a dominant ("D") or a minor ("M") lithology in the core, and the estimated percentages of sand, silt, and clay, together with all identified components.

SEDIMENTOLOGY

Classification of Sediments and Sedimentary Rocks

Leg 146 used a modified version of the sediment classification scheme of the Ocean Drilling Program (Shipboard Scientific Party, 1990b; Mazzullo et al., 1987) for granular sediment types (Fig. 7). Variations in the relative proportions of pelagic, neritic, siliciclastic, and volcanoclastic grain types define four major classes of granular sediments. Pelagic grains are the skeletal remains of open-marine siliceous and calcareous microfauna and microflora (e.g., radiolarians, diatoms, planktonic foraminifers, nannofossils) and associated organisms. Siliciclastic grains are mineral and rock fragments derived from igneous (plutonic and volcanic), sedimentary, and metamorphic rocks. Volcanoclastic grains include those of pyroclastic (direct products of magma degassing) and epiclastic (detritus derived from erosion of volcanic rocks) origins.

A granular sediment is classified by designating a principal name and major and minor modifiers. The principal name of a granular sediment defines its granular-sediment class; the major and minor modifiers describe the texture, composition, and fabric.

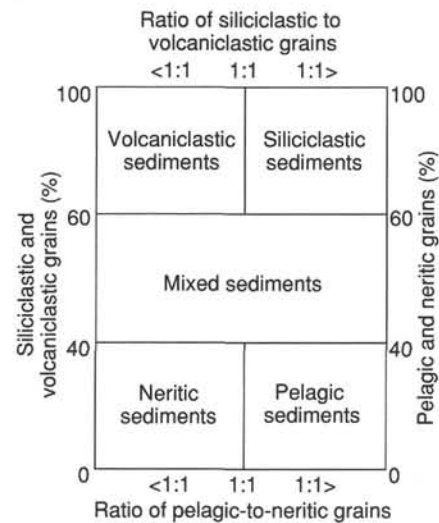


Figure 7. Diagram showing classes of granular sediment (modified from Mazzullo et al., 1987).

Principal Names

For siliciclastic sediments, the principal name describes the texture and is assigned according to the following guidelines:

1. The Udden-Wentworth grain-size scale (Wentworth, 1922; Fig. 8) defines grain-size ranges and names of the textural groups (gravel, sand, silt, and clay) and subgroups (fine sand, coarse silt, etc.) that are used as the principal names of siliciclastic sediment.
2. Principal names are listed in order of increasing abundance if two or more textural groups or subgroups are present in a siliciclastic sediment (Shepard, 1954; Fig. 9). For simplicity, we have grouped intermediate mixtures of the three textural end members—sand, silt, and clay—into four categories as shown in Figure 9 (i.e., sandy clay/clayey sand, silty clay/clayey silt, silty sand/sandy silt, and sandy silty clay).
3. The suffix "-stone" is affixed to the principal names sand, silt, and clay if the sediment is lithified. Conglomerate and breccia are used as principal names of lithified gravels with well-rounded and angular clasts, respectively.

Millimeters	Phi (ϕ)	Wentworth size class	
4096	-12.0	Boulder	Gravel
256	-8.0	Cobble	
84	-6.0	Pebble	
4	-2.0	Granule	
2.00	-1.0	Very coarse sand	
1.00	0.0	Coarse sand	Sand
1/2	0.50	Medium sand	
1/4	0.25	Fine sand	
1/8	0.125	Very fine sand	
1/16	0.0625	Coarse silt	Mud
1/32	0.031	Medium silt	
1/64	0.0156	Fine silt	
1/128	0.0078	Very fine silt	
1/256	0.0039	Clay	
0.00006	14.0		

Figure 8. Udden-Wentworth grain-size scale for siliciclastic sediments (Wentworth, 1922).

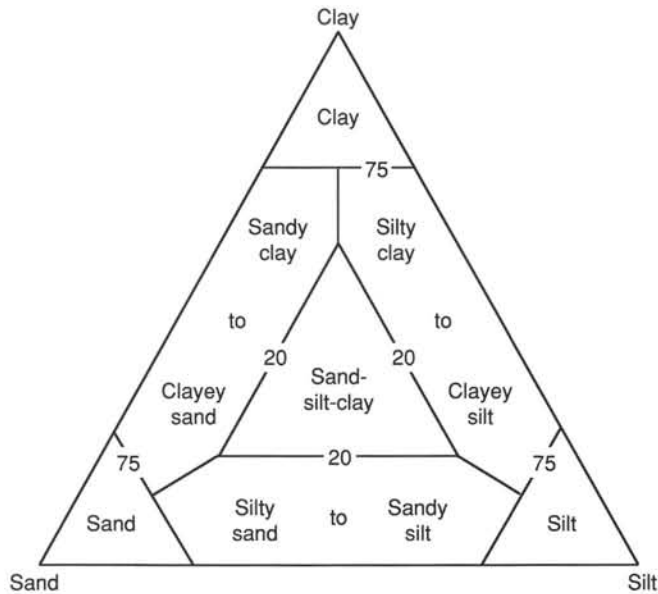


Figure 9. Ternary diagram showing principal names for siliciclastic sediments (modified from Shepard, 1954).

For Leg 146, volcanoclastic sediments are subdivided into two groups, pyroclastic and epiclastic, with the principal name in each group describing the texture. The names and ranges of the three textural groups for pyroclastic sediments/rocks (Fisher and Schmincke, 1984) are as follows:

1. Volcanic breccia: pyroclasts >64 mm in diameter.
2. Volcanic lapilli: pyroclasts between 2 and 64 mm in diameter; if lithified, the name "lapillistone" is used.
3. Volcanic ash: pyroclasts <2 mm in diameter; if lithified, the name "tuff" is used.

Epiclastic sediments, like siliciclastic sediments, are classified based on grain texture according to the Udden-Wentworth grain-size scale. The textural principal name is preceded by the modifier "volcanoclastic" (e.g., volcanoclastic conglomerate, volcanoclastic sand). Other rules apply as listed previously for siliciclastic sediments.

For pelagic sediment, the principal name describes the composition and degree of consolidation using the following terms:

1. Ooze: unlithified calcareous and/or siliceous pelagic sediments.
2. Chalk: partially lithified pelagic sediment composed predominantly of calcareous pelagic grains.
3. Limestone: lithified pelagic sediment composed predominantly of calcareous pelagic grains.
4. Radiolarite, diatomite, and spiculite: partially lithified pelagic sediment composed predominantly of siliceous radiolarians, diatoms, and sponge spicules, respectively.

Major and Minor Modifiers

The principal name of a granular-sediment class is preceded by major modifiers and followed by minor modifiers (preceded by "with") that describe the lithology of the granular sediment in greater detail. Major and minor modifiers are used most commonly to describe the composition and texture of grain types present in major (>25%) and minor (10%–25%) proportions and to describe grain fabric (e.g., matrix-supported).

The composition of pelagic components can be described with the major and minor modifiers diatom(-aceous), radiolarian, spicule(-ar), siliceous, nannofossil, foraminifer(-al), and calcareous. The terms

siliceous and calcareous are used generally to describe sediments composed of siliceous or calcareous pelagic grains of mixed origins. Sediment fabric can be described by the major modifiers grain-supported or matrix-supported. Generally, fabric descriptors are applied only to gravels, conglomerates, and breccias.

The degree of consolidation is described using the following major modifiers: "unlithified" designates soft sediment that is readily deformable under the pressure of a finger, "partially lithified" designates firm sediment that is incompletely lithified, and "lithified" designates hard, cemented sediment that must be cut with a saw.

Grain shape is described by the major modifiers rounded, subrounded, subangular, and angular. Sediment color, determined either with the Munsell soil-color charts (1971) or with a color spectrophotometer (Minolta Model CM2002), can be employed as a major modifier.

Mixed sediments are described using major and minor modifiers indicating the composition and texture.

Grain-size Analysis

The grain size was identified mainly through smear slides. In addition, the Lasentec LAB-TEC 100 particle-size analyzer was used on Leg 146 to determine the percentage count of particles in the size range of 0.004–0.25 mm. The percentage count passing through a laser beam in a liquid suspension was translated into weight percentage by the introduction of compensation factors.

X-ray Diffraction Methods for Fine Fractions

The fine fraction of selected samples was analyzed on board using X-ray diffraction (XRD) techniques. Sediments were put into suspension, and the fine fraction (less than 0.001 mm) was separated using a decantation method. The upper 5–7 cm of suspended material was removed after 24 hr, concentrated to a paste, and smeared on glass slides to produce oriented grain mounts. The slides were then allowed to air-dry. The XRD patterns of these oriented specimens were produced using the shipboard Philips AD 3420 X-ray diffractometer (Cu K α emission). After this initial analysis, each sample was treated with ethylene glycol, reanalyzed, then heated at 550°C for 1 to 1.5 hr, and again reanalyzed. Peaks were visually inspected and matched to standard reference peaks for various minerals (quartz, feldspar, hornblende, calcite, pyrite, clay minerals, etc.). Semiquantitative analysis of the relative proportions of clay minerals in the fine fraction was made using a peak-height method outlined by Biscaye (1964):

$$\text{smectite (17 \AA)/illite (10 \AA)/(chlorite + kaolinite) (7 \AA)} = 1/4/2.$$

BIOSTRATIGRAPHY

Time Scale/Chronological Framework

Two microfossil groups were examined for biostratigraphic purposes on Leg 146: radiolarians and planktonic foraminifers. Diatoms recovered on Leg 146 will be examined during post-cruise analyses. Age assignments were made primarily from core-catcher samples. However, additional samples from within the core were studied when a core-catcher sample was found to be inconclusive or otherwise unrepresentative of the core in its entirety.

Because Leg 146 used the Cande and Kent (1992) geomagnetic polarity time scale, ages for biostratigraphic datums that had been calibrated to the Berggren et al. (1985) time scale had to be converted. This conversion was usually straightforward, involving linear interpolation of the placement of each datum within the revised age boundaries of the magnetic polarity chron in which it falls. Figure 10 illustrates the correlation of the foraminifer and radiolarian zones to the geomagnetic polarity time scale of Cande and Kent (1992). The Miocene/Pliocene boundary was not defined because no sediments older than the Pliocene were expected to be recovered.

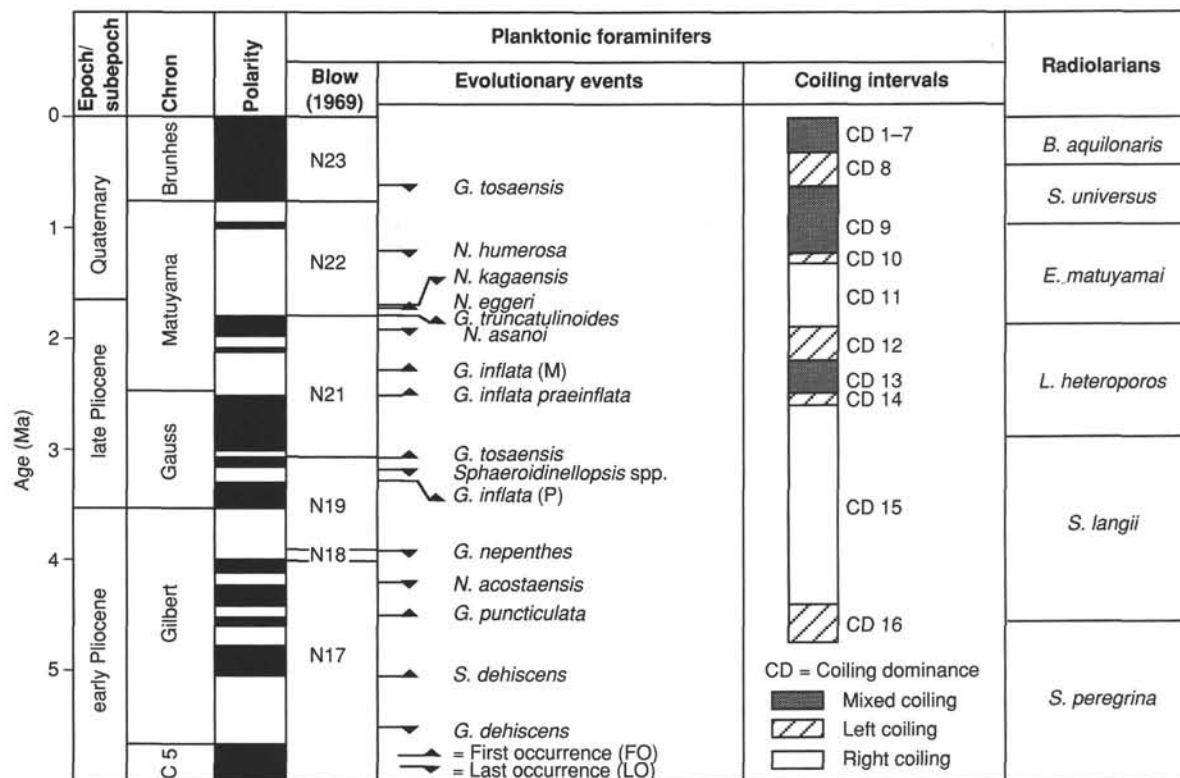


Figure 10. Correlation of radiolarian zones, planktonic foraminifer zonation of Blow (1969), planktonic foraminifer evolutionary events, and coiling zones of *Neogloboquadrina pachyderma* used on Leg 146 (see text) to the geomagnetic polarity time scale of Cande and Kent (1992).

In the following sections for foraminifers and radiolarians, ages of biostratigraphically useful datums are given for both the Cande and Kent (1992) and Berggren et al. (1985) geomagnetic polarity time scales. The source of correlation of the individual datums to the magnetic polarity chrons is also given.

Biostratigraphy/Paleoenvironments

Foraminifers

Chronological Framework

Direct application of mid- and low-latitude zonations such as that of Blow (1969) is often difficult or inappropriate for the northeast Pacific Ocean because of the temperate nature of the faunas. Therefore, foraminifer age determinations on Leg 146 were constrained by the chronostratigraphic framework developed by Lagoe and Thompson (1988) for the temperate North Pacific (Fig. 10). This framework was based on planktonic foraminifer evolutionary datums (first and last occurrences) and paleoclimatically controlled coiling shifts in *Neogloboquadrina pachyderma* (Table 1) from more than 20 locations in the North Pacific Ocean (see Lagoe and Thompson, 1988, for explanation). Lagoe and Thompson (1988) constructed a generalized coiling curve for the northeastern Pacific containing 16 correlative coiling intervals (CD = coiling dominance, Fig. 10). For shipboard purposes, the CD1–CD7 intervals of Lagoe and Thompson were grouped to represent a zone of high-frequency coiling shifts with mixed coiling directions from 367 ka to the present. Age determinations based on foraminifers are improved by integrating the coiling shifts with the zonation of Blow (1969).

Methods

Sediment samples of approximately 20 cm³ were taken from each core catcher. They were disaggregated in a Calgon solution and then

washed with tap water over a 63- μ m sieve. Residues were filtered and dried in an oven or under a heat lamp and dry sieved over a 149- μ m sieve. Fossiliferous samples were split with a microsplitter to obtain at least 300 specimens. Poor samples were picked out totally. Age assignments are made primarily on core-catcher samples.

Three classes of foraminifer preservation were used:

P = poor (almost all specimens were fragmented and showed evidence of dissolution and/or recrystallization).

M = moderate (30%–90% of the specimens were fragmented or showed evidence of dissolution/or recrystallization).

G = good (>90% of the specimens were unbroken and well preserved).

Planktonic foraminifer abundance was defined as follows:

R = rare (<10 specimens/20 cm³).

F = few (10–100 specimens/20 cm³).

C = common (101–500 specimens/20 cm³).

A = abundant (>500 specimens/20 cm³).

Benthic foraminifer abundance was defined as follows:

R = rare (<10 specimens/20 cm³).

C = common (10–100 specimens/20 cm³).

A = abundant (>100 specimens/20 cm³).

Paleoenvironmental Analysis

Benthic foraminifers were examined in the >149- μ m size fraction primarily for paleoenvironmental analysis (water mass properties) and interpretation of paleobathymetry. Paleobathymetric zonation was based on Ingle (1980) as follows: neritic (0–150 m), upper bathyal (150–500 m), middle bathyal (500–2000 m), lower bathyal (2000–4000 m), and abyssal (4000–6000 m).

Table 1. Ages of events in the chronostratigraphic framework of Lagoe and Thompson (1988), converted to the time scale of Cande and Kent (1992).

Event		Age ^a (Ma)	Age ^b (Ma)
	CD1-7/CD8 boundary	0.37	0.37
	CD8/CD9 boundary	0.6	0.6
F1	LO <i>Globorotalia tosaensis</i>	0.6	0.6
F2	LO <i>Neogloboquadrina humerosa</i>	1.1	1.2
	CD9/CD10 boundary	1.15	1.23
	CD10/CD11 boundary	1.3	1.4
F3	LO <i>Neogloboquadrina kagaensis</i>	1.6	1.7
F4	FO <i>Neogloboquadrina eggeri</i>	1.66	1.76
F5	FO <i>Globorotalia truncatulinoides</i>	1.7	1.8
	CD11/CD12 boundary	1.8	1.9
F6	LO <i>Neogloboquadrina asanoi</i>	1.85	1.9
	CD 12/CD13 boundary	2.1	2.2
F7	FO <i>Globorotalia inflata</i> (modern form)	2.2	2.4
	CD13/CD14 boundary	2.4	2.5
	CD14/CD15 boundary	2.5	2.6
F8	FO <i>Globorotalia inflata praeinflata</i>	2.5	2.6
F9	FO <i>Globorotalia tosaensis</i>	3.0	3.1
F10	LO <i>Sphaeroidinellopsis</i> spp.	3.1	3.2
F11	FO <i>Globorotalia inflata</i> (primitive form)	3.2	3.3
F12	LO <i>Globigerina nepenthes</i>	3.7	3.9
F13	LO <i>Neogloboquadrina acostaensis</i>	4.0	4.2
	CD15/CD16 boundary	4.2	4.4
F14	FO <i>Globorotalia puncticulata</i>	4.4	4.6
F15	FO <i>Sphaeroidinella dehiscens</i>	4.7	5.0
F16	LO <i>Globoquadrina dehiscens</i>	5.2	5.3

Note: CD = Coiling dominance intervals of Lagoe and Thompson (1988) for even (left coiling), odd (right coiling), and CD1-7 (high-frequency mixed coiling interval); FO = first occurrence; LO = last occurrence.

^a Estimated using the time scale of Berggren et al. (1985).

^b Estimated using the time scale of Cande and Kent (1992).

Radiolarians

Zonation

The Neogene radiolarian zonation (Fig. 10) follows the zonation of the Leg 145 Shipboard Scientific Party (Basov, Rea, Janecek, et al., in press) constructed mainly from the work of Hays (1970), Kling (1973), Foreman (1975), Riedel and Sanfilippo (1970, 1971, 1978), and Morley (1985). Radiolarian zones are defined as follows:

Botryostrobus aquilonaris Zone, Hays, 1970: the base is defined by the last occurrence of *Stylatractus universus*. This zone extends to the top of recent sediments.

Stylatractus universus Zone, Hays, 1970: the base is defined by the last occurrence of *Eucyrtidium matuyamai*.

Eucyrtidium matuyamai Zone, Hays, 1970; emend. Foreman, 1975: the base is defined by the first occurrence of *E. matuyamai*.

Lamprocyrtis heteroporos Zone, Hays, 1970; emend. Foreman, 1975: the base is defined by the last occurrence of *Stichocorys peregriana*.

Sphaeropyle langii Zone, Foreman, 1975: the base is defined by the first appearance of *S. langii*.

Stichocorys peregriana Zone, Riedel and Sanfilippo, 1970; emend. Foreman, 1975: the base is defined by the first evolutionary appearance of *S. peregriana*.

Table 2 lists radiolarian species events, many of which can be applied to North Pacific Cenozoic sediments, with ages based on the Cande and Kent (1992) geomagnetic time scale.

Methods

Sample preparation for microscopic examination during Leg 146 followed the standard techniques described by Sanfilippo et al. (1985). Samples were sieved first at 80 μ m to eliminate clay aggregates. A second mesh of 50 μ m was used for control.

For each sample examined, qualitative estimates of radiolarian abundance and preservation were made.

Table 2. Ages of Neogene radiolarian datum levels based on the Berggren et al. (1985) and Cande and Kent (1992) geomagnetic polarity time scales.

Event	Datum	Age ^a (Ma)	Age ^b (Ma)	Source of datum level ^c
R1	LO <i>Lychnocanoma grande</i>	0.05	0.05	1
R2	LO <i>Drupptractus acquiloni</i>	0.33	0.35	1
R3	LO <i>Stylatractus universus</i>	0.425	0.45	2
R4	LO <i>Lamprocyrtis neoheteroporos</i>	0.61	0.64	3
R5	LO <i>Eucyrtidium matuyamai</i>	0.98	1.05	3
R6	LO <i>Lamprocyrtis heteroporos</i>	1	1.07	3
R7	LO <i>Pterocanium prismatium</i>	1.6	1.7	4
R8	FO <i>Eucyrtidium matuyamai</i>	1.8	1.9	3
R9	FO <i>Cycladophora davisiana</i>	2.7	2.8	5
R10	LO <i>Stichocorys peregriana</i>	2.8	2.9	3
R11	LO <i>Theocorythium trachelium</i>	2.8	2.9	3
R12	FO <i>Lamprocyrtis neoheteroporos</i>	2.9	3	4
R13	LO <i>Stichocorys delmontensis</i>	3.4	3.55	3
R14	FO <i>Lamprocyrtis heteroporos</i>	4.4	4.6	5
R15	FO <i>Sphaeropyle langii</i>	4.4	4.6	3
R16	LO <i>Didymocyrtis penultima</i>	6.4	6.8	3

^a Berggren et al. (1985).

^b Cande and Kent (1992).

^c 1 = Morley et al. (1982), 2 = Hays and Shackleton (1976), 3 = Morley (1985), 4 = Johnson et al. (1989), and 5 = Spencer-Cervato et al. (in press.)

Radiolarian assemblage abundance was assessed as follows:

A = abundant (>500 specimens on the slide).

C = common (100–500 specimens on the slide).

F = few (50–100 specimens on the slide).

R = rare (<50 specimens on the slide).

Preservation of the radiolarian assemblage was based on the following:

G (good) = no sign of dissolution with only minor fragmentation.

M (moderate) = evidence of moderate dissolution with obvious fragmentation.

P (poor) = signs of a high degree of dissolution with few intact specimens.

STRUCTURAL GEOLOGY

Structural geology was an important facet of visual core description on Leg 146. The priorities the structural geologists set were:

1. To document all structures in the core and to record evidence for the relative timing of the various structures and diagenetic events.

2. To record the orientation of all structures on the core face and wherever possible to orient these in three dimensions in the core reference frame.

3. To orient structural features in a geographic framework by applying Eastman-Whipstock and Tensor multishot tool data, Formation MicroScanner (FMS) data, and primary remanent magnetization orientations to correct the measurements made in the core reference frame.

4. To obtain evidence from the style, geometry, and microstructure of individual structures that may bear upon the processes and conditions of deformation and the finite strain which can be inferred.

5. To construct plausible models of the tectonic environment and deformation history from all of these data.

The orientation of structures was recorded on a working core description form adapted from those devised on Legs 131 and 141 (Taira, Hill, Firth, et al., 1991, and Behrmann, Lewis, Musgrave, et al., 1992, respectively) and on a computer spreadsheet that allows manipulation and storage of the data. When more detailed graphical information about individual core sections was warranted, a structural VCD form was used to sketch individual structures (Fig. 11). The layout of these forms evolved during usage; examples of the final

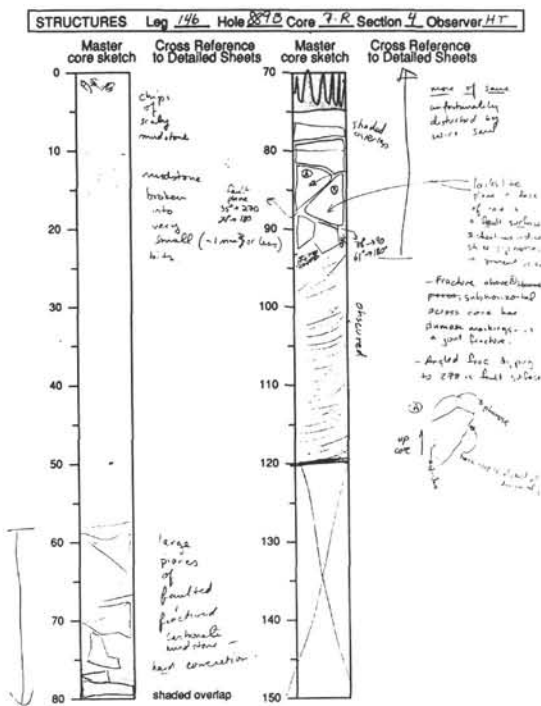


Figure 11. Structural visual core description form (VCD) used to record location and geometry of structures to scale.

versions are illustrated in Figures 11, 12, and 13. Where space and scale on the VCD were inadequate, the right-hand column of the description form was used for sketching and recording the geometries of important structures. The left-hand columns of the description form and the spreadsheet are more rigorously defined, prompting consistent and quantitative recording of the data, although the final format of these columns developed as the relative importance of various structural features in this setting became clear.

Description and Measurement of the Structures

A fundamental aspect of core description is recording of the orientation of the structures. However, relating orientations as seen in the cores to their actual subsurface disposition has long been a major problem, and this continued to be a difficulty on Leg 146. Endeavors to deduce the real orientation of structures required two stages; first, structures were oriented relative to some "local" reference coordinates, and second, this arbitrary reference frame was related to true north (when possible) and to true vertical. In general, the first stage can be done routinely, although it does require collecting and converting a large number of apparent orientation measurements. The system we used for these conversions is outlined in the following. The second stage depends on the availability of multishot, paleomagnetic, or FMS data, and was not possible for the majority of structural measurements on Leg 146.

The description and measurement of structures were based on the face of the archive half of the split core, though frequent recourse was made to the working half for additional information. The location of a structure was recorded in centimeters from the top of the section, according to conventional ODP procedure. Where a structure extended over an interval, the locations of the top and bottom of its range were recorded.

In an attempt to achieve consistency of nomenclature, the structural geologists defined descriptive terminology for macroscopic features, defined in the site chapters. There is no implication that these features fall into distinct pigeonholes; clearly, some gradation and

even overlap occurs. This natural variation was defined by adding modifiers, descriptive comments, and sketches. The description form allowed the recording of subtle variations in macroscopic appearance, but within a defined framework. The terminology has evolved from the experience of workers on previous DSDP and ODP legs.

A continuing problem was the distinction between natural structures and those caused by disturbance during coring and splitting. Another problem was that of recognizing structures developed during core recovery through stress release, desiccation, fluid expansion, and other processes. Planar structures with polished surfaces and/or linear grooves were regarded as tectonic rather than drilling induced, but the origin of zones of brecciation and gouge posed a problem. Features were not recorded if a tectonic origin was in doubt. In general, the recommendations of Lundberg and Moore (1986, pp. 42-43) were followed.

The dip of all structures exposed in the split cores was recorded according to the convention shown in Figure 14, that is, a two-digit angle between 0° and 90° for the apparent dip, together with an azimuth for the direction of the apparent dip (either 90° or 270°). Note that dips were recorded at this stage on the assumption that the long axis of the core is vertical, that is, deviations of the drill hole from vertical are ignored.

Attempts were normally made to establish the true dip of the structures. Typically, a second apparent dip was measured in a plane at a right angle to the core face. To do this the corresponding part of the structure was located on the working half of the core, and an incision was made parallel to the core axis. When identified, the apparent dip was marked by inserting a toothpick parallel to the feature on the incised surface and parallel to a plane bisecting the working half of the core (Fig. 14). This apparent dip was measured with a specially adapted protractor, and an azimuth of either 180° (dipping into the working half) or 0° (dipping away from the working half) was recorded. These data were used to calculate true dips in the core reference frame by stereographic projection, using the stereonet plotting program of R.W. Allmendinger, Version 4.1-11, on a Macintosh computer. The two apparent dip orientations were entered as lines, and the program found the great circle of cylindrical best fit to both lines. The orientation of this great circle gave the true orientation in the core reference frame of the observed structure, which was recorded on the description form and also entered into the spreadsheet. Where a structure was seen as a three-dimensional plane in a fragmented piece of core, or its trace could be observed at the top or bottom of a core section, it was possible to measure the true orientation directly in the core reference frame. In the adopted convention shown in Figure 14, 000° (a "pseudo-north") is the direction that splits the archive half at a right angle from the exposed face to the single line on the core liner. Because the structural descriptions are based on the archive half of the core, it was found more convenient to define the reference frame with respect to that half rather than to the double line on the working half, which defines the x -axis (0°) in the ODP paleomagnetic convention.

At the top and bottom of the core and on broken pieces, it was occasionally possible to discern linear structures such as the hairline grooves associated with faults and deformation bands, called here slickenlines. The orientation of these lineations was recorded. The sense and magnitude of fault separation were recorded as they appeared on the core face or on the top of broken pieces. Dip-slip separations and magnitudes were measured on the core face, and referred to as normal or reverse movements.

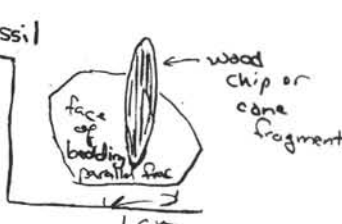
Our measurements of the orientations of structures observed in the cores were facilitated by a simple tool suggested by Neil Lundberg. A more detailed description of the tool and its use can be found in the "Explanatory Notes" chapter of the Leg 131 *Initial Reports* volume (Taira, Hill, Firth, et al., 1991). The device is illustrated in Figure 15A. It is a protractor-like graduated scale, with a pivoted measuring arm. During measurement, one half of the arm is aligned closely against the structure of interest and the other half points to the value of the dip angle on the graduated scale.

LEG 146 STRUCTURAL DATA: Working Core Sheets.

Elev		Core		HT		Observer		Comments					
287A		41X						Large intact pieces.					
section	cut from top		X-Ref	Identifier	Core Face Orientation		2nd. App. Orientation		Calc Orientation		W	↑ UP CORE	E
	top	bottom			App Dip	Direction	App Dip	Direction	Core Ref Frame	Geog Ref Frame			
2	103	106		Frac	9°	090	15°	180	59, 17S				
2	103	106		Brd (?)	9°	090	51°	000	277, 51N				
2	112	114		Frac.	21°	090	37°	180	63, 40S				
2	28	31		Frac	33°	270	41	000	253, 47N				
2	44	53		Frac	68	270	54	180	151, 71W				
3	99	101		Frac	26	090	7°	000	346, 27E				
3	99	101		LIN	23	090	43	000					
3	100	103		FRAC	5.1	270	70	180	114, 72S				
3	100	103		LIN	70 to 180								
4	0	14		FRAC	68	270	50	180	154, 70W				
4	56	65		FRAC	62°	270	30	180	163, 63W				
4	12	67		FRAC	48	270	0	180	180, 48W				
4	16	18		DEF BAND	74	270	20	000	186, 74W				

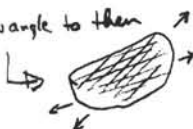
- Bedding plane(?) fracture with piece of wood in it. Was disturbed, but placed back in core by lining up fracture plane measured above. No clear lineation on this plane.

→ Dominant fracture in the fabric here at this interval



→ 23° plunge to ~120° lineation on above fracture. Forms set w/ lineated frac above. DOWN DIP LIN. ON ABOVE FRAC.

→ faint down dip slickenlines present; also as set at low angle to them



- dark seams parallel to fabric in adjacent broken-up zone

Figure 12. An example of the working core description sheet found useful for recording structural features.

Hole 889A																		
core	section	cm from top		mbsf	X-Ref Hand Sheets	Photo?	ID	identifier	Core Face Orientation		Corrected Core Ref Frame			Reorient Method	Corrected Geographic Ref Frame			Comments
		top	bottom						App Dip	Direction	Strike	Dip	Dir		Strike	Dip	Dir	
1	3	147	149					Bedding	13	270								Maybe drill deformation
1	6	51						Bedding	13	270	163	14 w	tensor	161.5	14 w			
1	4	46						Bedding	2	270								
1	3	130						Gas escape fracture	15	270								Gas escape feature. hackly parting surfaces
2	2	41						Bedding	0	0	0	0		33	0			horizontal bedding
2	6	70						Bedding	3	270								horizontal bedding
6	3	93						Bedding	11	90	48	16 s	tensor	276	16 n			
6	4	30						Bedding	11	90	62	24 s	tensor	290	24 n			
9	2	65	66					Bedding	4	270	180	4						loaded bed
9	2	91						Bedding	2	90	0	2						
9	6	70	71					Bedding	7	90	8	7						subhorizontal
9	8	60	63					Bedding	23	90	20	24						sketchy
10	1	60	76					Bedding	71	270								
10	2	102	112					Bedding	71	270	149	74 w	multishot	160	74 w			
10	3	55	67					Bedding	66	270								
10	5	91	101					Bedding	57	270	203	59 w	multishot	214	59 w			
11	1	45	50					Bedding	43	90	310	55 n	multishot	145	55 sw			
12	3	46	49					Bedding	36	270	172	36 w	tensor	238	36 n			
12	4	4	8					Bedding	38	270	126	53 s	tensor	192	53 w			
12	4	40	50					color change	54	90								at a high angle to apparent bedding
18	3	102	112					fracture	72	90								next 3 are coexisting joint sets
18	3	102	112					fracture	18	90								
18	3	102	112					fracture	65	270								
18	3	125	130					fracture	70	270								
18	3	140	147					fracture	60	270								pair of joints in fractured unit
18	3	140	147					fracture	65	90								
18	3	116	120					fracture	48	90	25	51						moderate lithif.; fracturing well developed
18	4	50	52					fracture	41	270	194	42						
18	4	10	18					fracture	75	90								pair of joints
18	4	10	18					fracture	50	270								
19	4	10	20					fracture	60	90								joints in fractured unit
19	4	45	50					fracture	45	90								
19	4	118						fracture	20	90	67	43						fairly indurated
19	4	130	145					fracture	60	90								
20	3	96	100					color change	46	90								irregular in x-section, no plane identified
20	3	45						interfrac angle	107									
20	4	110	115					fracture	61	90	330	64						scaly frac surface
20	4	80	85					fracture	50	90	328	55						conjugate present, but more poorly developed
22	2	15						fracture	27	90	316	35 e						set of apparently tectonic fractures
22	2	45						fracture	88	90	0	88 e						exhibit polished surface, undulose, faint slicks
22	6	51						fracture	19	270	248	43 n						excavated fracture
22	6	51						joint/fracture	43	90	15	44 e						pair of drill induced conjugates?
22	6	52						joint/fracture	50	270	199	52 w						" "
22	6	123	130					fracture	64	270	226	71 n						steep fracture near plane of cut face
22	6	123	130					lineation			T: 135	P: 16						weakly developed slicks on fracture surface
																		near strike-parallel
22	5	75						joint/frac	59	90	3	69 e						no slicks; fresh fracs
22	5	75						joint/frac	14	270	180	14 w						" "
22	5	75						joint/frac	66	90	40	71 w						" "

Figure 13. An example of the spreadsheet devised for the computer storage and manipulation of structural data derived from the core descriptions.

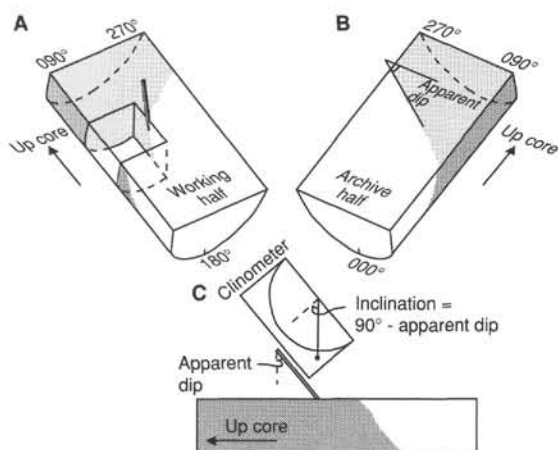


Figure 14. Diagram to show the conventions used for measuring azimuths and dips of structural features in cores and the techniques adopted for measuring structural planes in three dimensions in the core reference frame. The core reference frame conventions for the working half and the archive half of the core can be seen in Figures 14A and 14B. The E-W (core reference frame) apparent dip of a feature was measured first, generally on the face of the archive half (Fig. 14B). The data were recorded as an apparent dip toward either 090° or 270°. In this case the apparent dip is toward 090°. A second apparent dip is measured by making a cut parallel to the core axis but perpendicular to the core face in the working half of the core (Fig. 14A). Note that cuts were normally considerably smaller than the one represented in the diagram. The feature is identified on the new surface and the apparent dip in the N-S direction (core reference frame) marked with a toothpick. The apparent dip is measured with a modified protractor (Fig. 14C) and quoted as a value toward either 000° or 180°. In this case, the apparent dip is toward 180° (into the working half). True dip and strike of the surface in the core reference frame are calculated from the two apparent measurements.

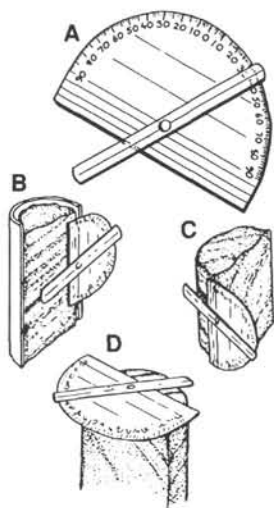


Figure 15. A. Drawing of a device for measurement of core-structure orientations. B. Device being used to measure the dip of a structure on the face of a split core. C. Device being used to assess the dip of a structure as seen at right-angles to the split-core face. D. Measuring the azimuth of a structure as seen on an upper surface of a core.

Figure 15B shows the device being used to measure the apparent dip angle of a structure on a split-core face, a common application. Dip angles refer, by definition, to inclinations from the horizontal, but there is no horizontal datum on a core; rather, it is the vertical axis, the length of the core, that forms the obvious datum. The baseline of the device is therefore aligned vertically. With the device in this alignment, the

arrangement of the graduated scale is such that when the measuring arm is rotated from horizontal to vertical the readings increase from 0° to 90°. Note that this is the opposite arrangement from that found on a conventional protractor. As suggested herein, the device therefore reads the dip angles directly, eliminating the mental arithmetic necessary if it is constructed from an ordinary protractor.

The advantages of this tool apply equally to measuring a dip angle at a right angle to the core face (Fig. 15C) or on some surface along which the core has broken.

A further application of the tool is the measuring of azimuths (Fig. 15D). The base line of the device is aligned parallel with the split-core face, and the arm is used to measure an azimuth. The arrangement of the scale is correct for the core reference frame used on Leg 146, provided the azimuths fall in the "northeast" quadrant; those falling in the "northwest" quadrant require the reading to be subtracted from 360°.

Real Orientation of the Structures

It was only possible to convert a limited number of the core reference frame orientations into true geographic coordinates. The lack of measurements of remanent magnetization, except at Site 889, generally limited such reorientation to APC cores. Data from the Eastman-Whipstock and Tensor multishot tools allow piston cores to be oriented with respect to magnetic north, and hence the arbitrary local reference frame to be positioned. The direction of permanent remanent magnetism in discrete samples was used to orient short intervals at Site 889. This technique was especially useful for cores obtained by RCB and XCB drilling because these techniques often cause the core to break into several pieces that rotate independently of each other within the core liner. In order to remove these drilling-induced rotations, remanent magnetization information was gathered from intervals of core that were considered to be structurally continuous, that is, rotated as a single piece. With the aid of the on-board paleomagnetic specialists, we found it possible to apply this information to the structural measurements. This method provided the declination and inclination of the natural remanent magnetism in the sample, which could then be used to orient the structures. Multishot studies indicate that deviations of the borehole from vertical were consistently less than 4° and hence could be neglected. The details of orientation methods used for specific cores are discussed in the site chapters.

True Position of the Structures

The depths in meters below seafloor on the spreadsheet are the values assigned to the core according to ODP convention. Core-log adjustment for the absolute depth of individual pieces depends on the availability of FMS data, and was not possible on the ship; conversion to reliable depth profiles requires complex processing, which at present cannot be conducted during a drilling leg.

The various corrections to orientations and positions that were possible on board ship have led to the structural syntheses presented in the site descriptions. Some of the interpretations will be refined following shore-based analysis of structural samples. An array of instrumental and analytical techniques will be employed to explore the nature of the structures in detail. The shipboard emphasis was on thorough and careful description of the range of structures observed.

PALEOMAGNETISM

Laboratory Facilities

The paleomagnetic laboratory on *JOIDES Resolution* is equipped with two magnetometers: a pass-through cryogenic superconducting rock magnetometer manufactured by 2-G Enterprises (Model 760R) and a Molspin spinner magnetometer. For Leg 146 an automatic ring-core fluxgate spinner magnetometer (designed by N. Niitsuma) and a Sapphire Instruments SI-2 anisotropy of magnetic susceptibility (AMS) device were also available on board. The laboratory has an

alternating field (AF) demagnetizer and a thermal demagnetizer (Models GSD-1 and TSD-1 by the Schonstedt Instrument Co.) capable of demagnetizing discrete specimens to 100 mT and 700°C, respectively. Partial anhysteretic remanent magnetization (pARM) can be imparted to discrete samples by a DTECH, Inc., PARM-2 system, consisting of two parallel coils mounted outside and on-axis with the AF-coil of the GSD-1 demagnetizer, and a control box. This device allows a bias field to be applied to a sample during AF demagnetization; the bias field can be switched on only over a window of AF field intensity during the declining-field stage of the demagnetization cycle. In addition, there is an in-line AF demagnetizer, capable of 25 mT (2-G Model 2G600), included on the pass-through cryogenic magnetometer track for the demagnetization of continuous sections. Demagnetization of archive-half material was limited to 15 mT during Leg 146 by Information Handling Panel policy, which has since been reviewed. All demagnetization devices and magnetometers are shielded within μ -metal cylinders.

The sensing coils in the cryogenic magnetometer measure the magnetic signal over about a 20-cm interval, and the coils for each axis have slightly different response curves. The widths of the sensing regions correspond to about 200–300 cm³ of cored material, all of which contributes to the signal at the sensors. The large volume of core material within the sensing region permits accurate determination of the remanence for weakly magnetized samples, despite the relatively high background noise related to the motion of the ship. The practical limit on the resolution of natural remanence of the core samples is often imposed by the magnetization of the core liner itself (about 0.1 mA/m = 10^{-7} emu/cm³).

The pass-through cryogenic magnetometer and its AF demagnetizer are interfaced with an IBM PC-AT-compatible computer and are controlled by a BASIC program modified from the original SUPERMAG program provided by 2-G Enterprises. The current versions (CUBE 146 for discrete samples and MAG146 for split-core sections) of the SUPERMAG program were previously modified to compensate for end effects. To do so, the program divides the sensor output by the portion of the area under the response curves occupied by the core or sample. Modifications of the programs during Leg 146 include better scaling for the screen output of MAG146 and CUBE146 and the inclusion of AF levels from the GSD-1 in the CUBE146 data files. The spinner magnetometer used for measuring discrete samples was interfaced with a Macintosh SE30 computer with a program brought on board by D. Schneider (Woods Hole Oceanographic Institution) for Leg 138.

The ring-core fluxgate spinner magnetometer automatically demagnetizes samples with alternating fields up to 45 mT before being measured. It is also capable of measuring susceptibility and susceptibility anisotropy and of inducing anhysteretic remanent magnetization (ARM).

The SI-2 AMS device measures the low-field (0.1 mT) susceptibility of discrete paleomagnetic samples. The noise level of the SI-2 on board the ship is 3×10^{-6} (SI volume units); a susceptibility of greater than 1×10^{-4} is necessary for the accurate determination of a sample's magnetic anisotropy.

The magnetic susceptibility of unsplit sections of core is measured with a Bartington Instruments Model MS1 susceptibility meter adapted with a MS1/CX 80-mm whole-core sensor loop set at 0.465 kHz. The full width of the impulse response peak at half maximum is less than 5 cm. The susceptibility sensor is mounted with the GRAPE and P-wave logger on the MST. The susceptibility of discrete specimens can be measured on board with a sensor unit (type MS1B) attached to the Bartington susceptibility meter.

An Analytical Services Company Model IM-10 impulse magnetizer is also available in the magnetics laboratory for studies of the acquisition of both stepwise and saturation isothermal remanence magnetization (IRM) by discrete samples. This unit can apply pulsed fields from 20 to 1200 mT.

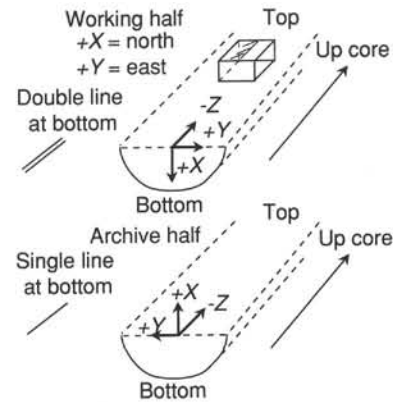


Figure 16. Paleomagnetic core orientation conventions for split-core sections and discrete samples.

Paleomagnetic Measurements

Pass-through Magnetometer

The bulk of the paleomagnetic measurements on Leg 146 was made with the pass-through cryogenic magnetometer. Pass-through paleomagnetic measurements were routinely performed on the archive halves of core sections. The ODP core orientation scheme arbitrarily designates the x -axis as the horizontal (in situ) axis radiating from the center of the core through the space between a double line inscribed lengthwise on the working half of each core liner (Fig. 16). The natural remanent magnetization (NRM) and remanence measurements after 5, 10, and/or 15 mT AF demagnetization were routinely measured at 5-cm intervals. Occasionally, the measuring interval of the NRM and the demagnetized remanence was increased to 10 cm. This was done when the magnetic signal was weak, and it was apparent that the magnetic polarity could not be resolved, or to accelerate core-flow through the laboratory.

The NRM was dominated generally by a vertical upward magnetization, presumably acquired during coring or recovery. Even so, the NRM measurements contain important information about the expected magnetization of the sediment and possibly the origin of the overprinting. The magnetostratigraphic interpretations for Leg 146 are based on both the pass-through measurements of the demagnetized cores and the results from discrete samples measured on either spinner magnetometer. Several intervals of core had overprints that could not be removed by the maximum (15 mT) AF level allowed for use on archive-half sections. For these intervals the magnetostratigraphy was based entirely on discrete sample data from the working half. Data from core segments that are clearly physically disturbed, such as within the more gas-rich cores, were deleted from the data files. Other segments of core that are magnetically noisy and uninterpretable or have an insufficient magnetic signal were also excluded from the shipboard analysis, but the data are retained in the primary ODP data files.

Low-field Susceptibility

Whole-core susceptibility measurements are made relatively rapidly, are nondestructive, and provide a rough indication of the amount of magnetizable material in the sediment, including ferrimagnetic and paramagnetic constituents. The instrument was set to the low sensitivity range (1.0) in the SI mode, and measurements were usually made every 5 cm, depending on the available time for on-board measurements. When the susceptibility decreased to a level indistinguishable from instrumental noise, the measurement interval was increased to 15 or 20 cm. The susceptibility data were archived in raw instrument meter readings. To convert these values to susceptibility units it is necessary to multiply by 0.63, calculated from the manufacturer's manual, to

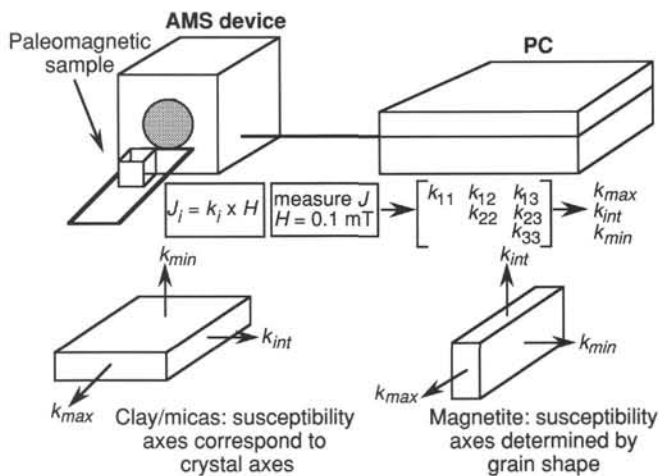


Figure 17. Schematic of anisotropy of magnetic susceptibility (AMS) procedure. From the value of induced magnetization (J) in a sample for a given applied field (H), the susceptibility (k_i) is determined. Using six orientations, the k_{ij} terms of the susceptibility matrix are measured, from which the principal susceptibility axes (k_{max} , k_{int} , k_{min}) are calculated. For clay/mica minerals and pyrrhotite, the principal susceptibility axes correspond to crystallographic axes, for magnetite the susceptibility axes correspond to dimensional axes of individual grains.

compensate for the 0.77 ratio of core diameter (68 mm) to coil diameter (88 mm). An additional multiplication factor of 10^{-5} is necessary to complete the conversion to volume-normalized SI. These factors were checked against the values expected for distilled water. The meter was zeroed with each section, but no correction was made on board for the instrumental baseline drift that occurred during the measurement of each section's susceptibility profile. However, the necessary parameters were recorded and will be processed on shore.

Magnetic Anisotropy

The AMS measurements were conducted on discrete samples to determine the geometry of the mineral fabrics found in the Leg 146 cores. The SI-2 device determines the magnetic anisotropy tensor from measurements of magnetic susceptibility in six orientations (Fig. 17), with the eigenvalues and eigenvectors of the tensor representing the magnitude and orientation of the principal susceptibility axes ($k_{max} > k_{int} > k_{min}$). For several samples the relative contributions of ferrimagnetic and paramagnetic minerals to the low-field susceptibility were determined using the cryogenic susceptibility method (Ihmlé et al., 1989). The analysis involves cooling a discrete sample in liquid nitrogen to 77 K, and measuring the bulk susceptibility as the sample heats to ambient temperature. A pure ferrimagnet has constant susceptibility as a function of temperature (below the Curie point), whereas a pure paramagnet has a susceptibility that is inversely proportional to temperature. Examination of the susceptibility vs. temperature behavior is used to quantify the ferrimagnetic and paramagnetic components of the low-field susceptibility.

Anhyseretic Remanence and Isothermal Remanence

Discrete samples, which had already been AF demagnetized, were exposed to a bias field of 0.1 mT while alternating fields were applied in increasing steps, and the resulting ARM was measured at each stage on either the Molspin magnetometer or the ring-core fluxgate spinner magnetometer. The bias field was applied parallel to the z -axis (down-core). Acquisition of ARM gives information about the alternating field coercivity spectrum of the samples, which clarifies the interpretation of AF-demagnetization behavior and helps identify the presence of separate populations of magnetic minerals. IRM was imparted

to samples in applied fields increasing in steps up to 1.2 T. Stepwise IRM acquisition can be used to distinguish between magnetite, which is saturated in applied fields greater than about 200 mT (Banerjee and O'Reilly, 1967; Ishikawa, 1967), and hematite, which commonly remains unsaturated in fields of 1.0 T and more. Magnetic iron sulfides (pyrrhotite and greigite) may also remain unsaturated until above 0.2 T (Kligfield and Channell, 1981; Musgrave et al., 1993). IRM acquisition may also distinguish the contribution of differing magnetic carriers or differing magnetic grain sizes over the coercivity interval less than 200 mT.

A further test of the combined thermal stability and IRM coercivity was accomplished by imparting a multicomponent IRM (mIRM) in fields of 0.2, 0.4, and 1.2 T along the x , y , and z sample axes in turn, and then thermally demagnetizing the samples (Lowrie, 1990). The mIRM technique allows for the identification of magnetic minerals through a combination of their coercivity and thermal stability properties, resolving ambiguous interpretations of magnetic mineralogy based on saturation IRM properties alone. Thermal demagnetization was initially conducted over 20°C steps from 40° to 100°C , allowing time for the sample to dry adequately. Thermal demagnetization then continued at 10° – 50°C steps to 650°C . Samples contained in plastic cubes were carefully removed for each thermal treatment; their plastic boxes were separately AF-demagnetized at each step and the samples returned to their boxes for measurement.

Core Orientation

Core orientation of APC cores was achieved with an Eastman-Whipstock multishot tool and the new Tensor multishot tool, either of which may be mounted on the core barrel. The Eastman-Whipstock tool consists of a magnetic compass and a camera. The battery-operated camera photographs continuously at predetermined intervals of from 0.5 to 2 min, beginning at the time it leaves the deck. At the bottom of the hole the core barrel is allowed to rest for sufficient time (2–8 min) to settle the compass needle and to make sure that several photographs are taken before the corer is shot into the sediment. The photographs used for orientation are those taken just prior to shooting the core barrel into the sediment.

The Tensor tool consists of three mutually perpendicular magnetic sensors and two perpendicular gravity sensors. The information from both sets of sensors allows the azimuth and dip of the hole to be measured as well as the azimuth of the APC core orientation double-line.

Orientation is not usually attempted for the top three cores (to about 30 mbsf), until the bottom hole assembly is sufficiently stabilized in the sediment. Core orientation by the multishot tools was generally successful during Leg 146, with a subjective accuracy estimate of 20° – 30° , and declinations oriented by this method contributed to the magnetostratigraphic interpretations. Exceptions to this typical performance are noted in the site chapters.

Magnetostratigraphy

Whenever possible in the site chapters we offer an interpretation of the magnetic polarity stratigraphy using the new magnetic polarity time scale of Cande and Kent (1992) (see Table 3). Two additional short geomagnetic features, observed with sufficient regularity that they may make useful stratigraphic markers for regional/global correlations, are the Blake feature at about 0.11 Ma in the Brunhes and the Cobb Mountain event at about 1.1 Ma. For the upper part of the time scale (roughly Pliocene-Pleistocene), we use the traditional names to refer to various chrons and subchrons (e.g., Gauss, Jaramillo).

ORGANIC GEOCHEMISTRY

The drilling objectives of Leg 146 include an extensive component of organic and inorganic geochemistry. Organic geochemical investigations are conducted to provide (1) real-time monitoring of volatile

Table 3. Geomagnetic time scale of Cande and Kent (1992).

Polarity chron	Age (Ma)
Brunhes/Matuyama	0.780
Termination Jaramillo	0.984
Onset Jaramillo	1.049
Termination Olduvai	1.757
Onset Olduvai	1.983
Termination Réunion	2.197
Onset Réunion	2.229
Matuyama/Gauss	2.600
Termination Kaena	3.054
Onset Kaena	3.127
Termination Mammoth	3.221
Onset Mammoth	3.325
Gauss/Gilbert	3.553
Termination Cochiti	4.033

hydrocarbons, hydrogen sulfide, and other gases as part of the shipboard safety requirements and (2) an initial characterization of the types, amounts, and maturity of the sedimentary organic matter and bitumens found. The analytical program was intended to provide preliminary geochemical information for additional or more detailed shore-based studies. The following instrumentation and procedures were used during Leg 146 to (1) measure the concentrations of hydrocarbon and other gases, (2) test for gas hydrates and fluid flow, (3) conduct analysis of high molecular weight hydrocarbons and long-chain alkenones in selected sediments, and (4) determine the quantity and quality of organic matter in the sediments.

Sampling for Headspace Gases

During Leg 146, the compositions and concentrations of hydrocarbons and other gases were monitored in the sediments generally at intervals of two per core. Two methods were used, called headspace (HS) and vacutainer (V).

In the HS method, gases released by the sediments after core recovery were analyzed by gas chromatography (GC) with the following technique: a modified (open-ended) 5-mL plastic syringe or a calibrated cork borer was used to obtain a measured volume of sediment from the end of a section of core, immediately after retrieval on deck. The sediment, usually about 5 cm³, was placed in a 21.5-cm³ glass serum vial that was sealed with a septum and metal crimp cap. When consolidated or lithified samples were encountered, chips of material were placed in the vial and sealed. The vial was then heated to 60°C in an oven and kept at this temperature for 30 min before gas analysis. A 5-cm³ volume of the headspace in the vial was extracted with a standard glass syringe for each analysis by gas chromatography.

The vacutainer method of gas analysis was used when gas pockets or expansion voids occurred in cores as they arrived on deck. Vacuainers are pre-evacuated, septum-sealed glass tubes (20 cm³). For the purpose of obtaining a gas sample, a special tool is employed to penetrate the core liner. This tool, equipped with a valve and needle, is used to transfer gas from the core into the vacutainer. Portions of gas in the vacutainer were analyzed by gas chromatography.

Hydrocarbon and Other Gases

Compositions and concentrations of hydrocarbon and other gases were monitored in the headspace and vacutainer samples, generally once per core, using two different gas chromatographic systems: (1) Hach-Carle AGC Series 100 (Model 211), referred to as HC, and (2) Hewlett-Packard 5890A, Natural Gas Analyzer, modified by John Booker & Company, Austin, Texas, and referred to as NGA.

Hach-Carle Gas Chromatograph

The Hach-Carle (HC) gas chromatograph is a standard packed-column flame ionization detector (FID) GC, the output of which is

attached to a Hewlett-Packard Model 3393A Integrator that allows the single measurement of gas concentrations over 6 orders of magnitude after appropriate calibration. The HC instrument is designed to measure accurately in about 7 min the concentrations of methane, ethane, and propane. Ethene is resolved from ethane and can also be quantified. The HC has the following characteristics: sample introduction is by means of a 1.0-cm³ sample loop with manual column backflush; the chromatographic columns used were a 0.32 cm × 1.8 m stainless-steel tubing packed with 80% Porapak N and Porapak Q (80/100 mesh) and a 0.32 cm × 1.8 m stainless-steel tubing packed with 10% Carbowax 20M on Chromasorb W-HP (80/100 mesh). Only the first column was used for routine analyses. For detection an FID was used and the chromatographic conditions were isothermal at 90°C, with helium used as the carrier gas.

Hewlett-Packard Gas Chromatograph (NGA)

The modified NGA is a modified multivalve, multicolumn gas chromatograph equipped with both a thermal conductivity detector (TCD) and an FID. Two Hewlett-Packard Model 3393A Integrators were dedicated to the TCD and FID. This GC analysis system consists of automatic valve switching to direct flows through various sample loops and columns. Three GC columns were used sequentially to provide a rapid partitioning and measurement of N₂, O₂, CO₂, H₂S, CS₂, and C₁ to C₇ hydrocarbons.

The modified NGA employs a multicolumn system composed of a 0.32 cm × 1.8 m stainless-steel column packed with Porapak T (50/80 mesh) in line with a 0.32 cm × 0.9 m column packed with Molecular Sieve 13X (60/80 mesh), a 0.32 cm × 1.8 m stainless-steel column packed with 80/100 mesh Haysep (acid washed), and a 60 m × 0.32 mm capillary column coated with a 1-μm film thickness of DB-1 (J&W Inc.). Samples were introduced by means of a 0.5-cm³ sample loop with an automatic sample backflush. The chromatographic separation on the TCD portion of the NGA system was carried out isothermally at 80°C, whereas the hydrocarbon separation on the FID portion was carried out by programming from 80° to 100°C at 8°C/min and then to 200°C at 30°C/min. Helium was used as the carrier gas. The TCD injector and detector temperatures were 80°C and 150°C, respectively, and the corresponding temperatures for FID were 150°C and 250°C, respectively. Chromatographic response was calibrated against preanalyzed standards and the gas contents are reported in ppm (v/v).

A more quantitative evaluation of the gas concentration was possible by relating the headspace volume and gas composition to the weight of the sediment sample. Weights were determined by difference with the preweighed vials.

Bitumen Analyses (C₁₅₊ Hydrocarbons and Alkenones)

Initial screening of sediment extracts was carried out on the *n*-hexane supernatant from the fluorescence extraction, which was removed and concentrated for analysis. Freeze-dried sediment samples were gently ground in an agate mortar, and about 500 mg of each was weighed out and transferred into 2-dram screw-capped vials. Normal hexane (*n*-C₆H₁₄, 2 mL) and methanol (CH₃OH, 2 mL) were added and the suspension shaken occasionally for about 2 hr. The clear supernatant solution was pipetted into a second vial and the extraction was repeated with another 1-mL aliquot of *n*-C₆H₁₄. The combined extract was evaporated to near dryness under nitrogen blow-down at about 40°C, then taken up in *n*-hexane to a volume of 50 μL. A 1- to 8-μL sample was then injected using normal GC protocol. Hydrocarbons were identified by comparison of the retention times with those of authentic standards. The final quantification of the results was based on the weight of dry sediment and the aliquot used in the injection. Solvent blanks and drilling greases were also analyzed.

Solvent-soluble organic material was analyzed by gas chromatography on the Hewlett-Packard Model 5890A GC, equipped with a

capillary column and split injection. Helium was used as the carrier gas. Operating conditions for this instrument were as follows:

1. Column: HP Ultra 1 (cross-linked methyl silicon gum), 50 m \times 0.2 mm \times 0.11 μ m film thickness.
2. Conditions: He, 400 kPa; air, 200 kPa; and H₂, 150 kPa.
3. Temperatures, injector, 250°C; detector, 300°C; temperature program, initial at 30°C for 3 min 10°C/min to 220°C, 4°C/min to 300°C, and then isothermal for 15 min.

Fluorescence

Fluorescence measurements can indicate the presence of aromatic compounds in petroleum and its products (e.g., Wyman and Castaño, 1974). Fluorescence of pyrolysis products (bitumen) is an approximate indicator of the evolution of the petroleum potential of a sediment. It reflects the aromaticity of the hydrocarbons in the bitumen (Kelts et al., 1982). Fluorescence data were measured on bulk-sediment samples taken from each core as *n*-hexane/methanol extract solutions. The fluorescence intensity was estimated under a UV lamp (Kelts et al., 1982).

Organic Matter

Organic Carbon

The total organic carbon content (TOC) of the sediments was determined by Rock-Eval TOC (explained in the following) or by the difference between carbonate carbon, determined with the Coulometrics Model 5030 Carbonate Carbon Apparatus, and the total carbon value, determined with the Carlo Erba Model NA 1500 NCS Analyzer. A description of the Coulometrics instrument and procedure can be found in the "Inorganic Geochemistry" section (this chapter).

Organic Matter Type (Pyrolysis Methods)

Two pyrolysis systems were available on Leg 146 to evaluate the quality and quantity of organic matter. The standard system is the Delsi-Nermag Rock-Eval II plus total organic carbon. A new system is the Geofina hydrocarbon meter (GHM). Both systems use a whole-rock pyrolysis technique to identify the type and maturity of organic matter and to detect petroleum potential and oil shows in sediments as described by Espitalié et al. (1985a, 1985b, 1986).

The Rock-Eval system involves a graduated temperature program that first releases volatile hydrocarbons at 300°C for 3 min, and then releases hydrocarbons from thermal cracking of kerogen as the temperature increases at 25°C/min from 300° to 600°C. Four parameters characterizing the organic matter are determined:

1. S₁: The amount of free hydrocarbons (bitumen) in the sample (mg hydrocarbons per g of rock) recorded at pyrolysis temperatures below 300°C.
2. S₂: The amount of hydrocarbons generated through thermal cracking of the kerogen as the sediment is heated at 25°C/min from 300° to 550°C during pyrolysis (cycle 1). S₂ is an indication of the quantity of hydrocarbons that could be produced in this rock, should burial and maturation continue.
3. S₃: The quantity of CO₂ (mg CO₂ per g of rock) produced from pyrolysis of the organic matter at temperatures between 300° and 390°C is detected by TCD and recorded during cooling.
4. T_{max}: Maturity of the organic material assessed by the temperature at which a maximum release of hydrocarbons from cracking of kerogen occurs during pyrolysis (top of the S₂ peak).

The Rock-Eval data can also be interpreted for type of organic matter by the hydrogen index [(100 \times S₂)/TOC], oxygen index [(100 \times S₃)/TOC] and the S₂/S₃ ratio. The first two parameters are normally referred to as HI and OI, respectively. Rock-Eval pyrolysis is consid-

ered to be unreliable for samples with less than 0.5% TOC (Katz, 1983; Peters, 1986), although a correction procedure has been described for estimating matrix effects and obtaining reliable values on samples with lower amounts of TOC (Espitalié, 1980).

The GHM is a GC system based on the Varian 3400 series gas chromatograph, which has been modified to include the GHM pyrolysis injector and corresponding valve configuration. The system employs three flame ionization detectors and two capillary columns (25 m, GC2 fused silica). The system determines S₁, the free hydrocarbons that are released from the injector at 300°C, and S₂, the pyrolysis products that are generated by ramping the temperature of the furnace from 300° to 540°C at 25°C/min. The effluent from the furnace is split 20:1 so that the hydrocarbon distributions making up S₁ and S₂ can be examined by capillary gas chromatography. The T_{max} value of the S₂ peak is also determined. Rock-Eval and GHM parameters are used to calculate the production index (PI) = S₂/(S₁ + S₂) and petroleum potential or pyrolyzed carbon (PC) = 0.083(S₁ + S₂). Sample size for both systems was typically 100 mg.

INORGANIC GEOCHEMISTRY

Interstitial water was obtained from sediments by squeezing and by in-situ extraction using the water-sampling temperature probe.

Interstitial Water Sampling

Interstitial waters were squeezed from whole-round sections of sediment cores 5 to 20 cm long which were cut from the cores as soon as they arrived on deck. Whole-round sections were taken from nearly every core, when recovery was sufficient. Sediment from whole-round sections was immediately extruded from the core liner, scraped with a stainless-steel spatula to remove the outer, contaminated layer, and placed in a titanium squeezer similar to the steel squeezer designed by Manheim and Sayles (1974). Sediments were squeezed in a Carver hydraulic press at pressures up to 30,000 lb. Interstitial water was collected directly from the squeezer into a 50-mL all-plastic syringe, from which the various aliquots for analysis were ejected through an on-line, 0.2- μ m, polysulfone filter mounted in a Gelman "acrodisc" disposable filter holder. No attempt was made to equilibrate the sample with the in-situ temperature before squeezing. Squeezed interstitial waters were designated IW samples.

In-situ Extraction

Interstitial water was extracted in situ with the WSTP tool (Barnes, 1988), which simultaneously measures sediment temperature (see "WSTP and ADARA Temperature Measurements" sections of the site chapters). The tool is lowered on the coring wire to the end of the drill string, where it locks onto an assembly just above the bit. While the tool descends, the hole is flushed with drilling fluid (usually surface seawater), with the bit just off bottom to keep the hole free of fill. After the sampler is latched into place, the bit is lowered into the bottom with the filter assembly projecting about 1.1 m past the bit. A time-operated valve opens and interstitial water is drawn under negative pressure through the filter and into the sampler.

The filter assembly has been lengthened to 22 cm and is narrower than in an earlier version of the tool. These modifications reduce fracturing of the formation and produce a filter surface area of 200 cm². A 1- μ m, polyester-mesh filter was sandwiched between two layers of 80- μ m, titanium screen that were held together with epoxy. After passing through the filter assembly, pore fluids enter the sample reservoir by means of 1/16-in. titanium tubing. The tube is held in a groove cut into a titanium sleeve that fits around the thermistor probe shaft. The sleeve, tubing, and filter are covered by a second titanium sleeve. This outer sleeve, which provides support and abrasion protection for the filter, is perforated approximately every centimeter with 0.5-cm holes to allow fluid to pass. The titanium tube holds less

than 4 mL of fluid and is connected to a titanium sample coil that holds approximately 6 mL of fluid. This in turn is connected to a stainless-steel sample coil that holds approximately 40 mL. Except for the stainless-steel coil, all of the connectors and valves are titanium or Teflon. A one-way valve is connected to the other end of the copper coil, which allows fluid to pass into a stainless-steel overflow cylinder. The overflow cylinder generates negative pressure when the sampling valve is open, because the cylinder is normally filled with air when the tool is sent downhole.

The procedure for fluid sampling with the WSTP is unchanged from that used during earlier legs. Before deployment the fluid path is back-filled with distilled water that was previously degassed by bubbling nitrogen. The overflow cylinder is flushed with nitrogen and evacuated. A timer is set for a fixed time after which the valve will open, exposing the sampling line and chamber to ambient pressure. The timer also closes the valve after a prearranged time interval has passed. The valve is kept open for about 15 min. The tool is recovered after the sample valve has closed.

When the tool is returned to the laboratory, the cover for the chamber containing the sample coils is carefully removed and any "overflow" water present is collected and designated as a "BO" sample. This fluid includes the distilled water that occupied the space inside the titanium tubing (6 mL) and the sample coils (54 mL) before deployment, plus all fluid in excess of 60 mL collected downhole. If a small fluid sample (<60 mL) is collected by the tool, the overflow fluid will be nearly all distilled water, and the sample will be diluted. If a large volume is collected (>60 mL), then the fluid trapped in the sample coils is from either the formation or the borehole. Fluids from the overflow cylinder were also analyzed, as they can be useful for determining the concentration of the major and minor species that are dissolved in pore waters. The amount of dilution of the overflow aliquot can usually be determined from its chlorinity relative to that of the undiluted sample. Whether the tool samples pristine, in-situ pore water depends on how deeply it is pressed into the formation, how permeable the sediments are, and whether the formation cracks during insertion of the probe.

Fluid from the titanium and stainless-steel sample coils was filtered (0.2 μm) and used for the determination of major and minor dissolved species. These samples were designated "Ti" and "SS," respectively.

Analytical Methods

Interstitial-fluid samples were analyzed immediately upon recovery for pH, alkalinity by potentiometric titration, and salinity by refractive index. Aliquots were refrigerated and analyzed within a few days for chlorinity, magnesium, and calcium by colorimetric titration; sulfate by ion chromatography turbidimetry; silica, phosphate, and ammonium by colorimetry; potassium and lithium by flame atomic emission; and strontium by atomic absorption spectrophotometry. Most shipboard analyses were performed using standard ODP techniques, as detailed by Gieskes et al. (1991). The techniques employed are summarized in Table 4. We used IAPSO as our primary standard for determination of calcium, magnesium, chlorinity, and sulfate. Other analyses employed reagent grade chemicals as suggested by Gieskes et al. (1991).

Carbon, Nitrogen, and Sulfur Analyses

Sediments were analyzed on-board ship for inorganic carbon and for total nitrogen, carbon, and sulfur. The TOC content of the sediments was then calculated by subtraction of the inorganic carbon content from the total carbon content. The analyses were carried out on sediment left in squeeze cakes, from which most of the interstitial waters had been removed by pressing in the titanium squeezers. The sediments were freeze-dried before being analyzed.

The total inorganic carbon was determined using a Coulometrics 5011 coulometer equipped with a system 140 carbonate carbon

analyzer. Approximately 5 mg of ground and weighed sediment was reacted in a 2N HCl solution. The liberated CO_2 was titrated in a monoethanolamine solution with a color indicator while the change in light transmittance was monitored with a photodetector cell.

Total nitrogen, carbon, and sulfur were determined using a NA 1500 Carlo Erba NCS analyzer. Bulk samples were combusted at 1000°C in an oxygen atmosphere with the addition of vanadium pentoxide, converting organic and inorganic carbon into CO_2 and sulfur into SO_2 . These gases along with nitrogen were then separated by gas chromatography and measured with a thermal conductivity detector.

PHYSICAL PROPERTIES

General Objectives

The standard procedures for shipboard measurement of physical properties were modified and substantially expanded to serve a number of objectives unique to Leg 146. The principal objectives for the physical properties group underlie the general themes of this cruise. They can be grouped together as follows:

1. To determine the mechanical state and deformation properties of the sediments,
2. To assess the hydrologic conditions, and
3. To estimate the in-situ stress.

To correlate shipboard and shore-based laboratory measurements with the in-situ state of stress and to better constrain existing thermo-mechanical models of fluid flow and deformation, the downhole tools ADARA (temperature), WSTP (water sampling and temperature measurement), Geoprops probe (water sampling, pore pressure, temperature, and permeability), and LAST-II (lateral stress, pore pressure, and strength) were deployed. Whole-round samples were extensively taken from APC/XCB-cored sections for onshore laboratory measurement of consolidation, permeability, triaxial testing and x-ray tomography.

Standard shipboard measurements of physical properties to document the evolution of sediment physical properties during the process of frontal accretion and imbrication include nondestructive, whole-core measurements made with the multisensor track (MST) (P -wave velocity, magnetic susceptibility, and gamma-ray attenuation), undrained shear strength, thermal conductivity, electrical resistivity, compressional wave velocity, and index properties. Sampling frequency for most parameters was significantly increased from standard shipboard procedures to resolve and correlate properties with other shipboard data, particularly with downhole geophysical logs. On average, one sample was selected every 70 cm, where recovery permitted. In good-quality core samples where the sample completely filled the liner, the MST sample frequency was one measurement every 1 cm for GRAPE, every 3 cm for magnetic susceptibility, and every 2 cm for P -wave velocity. To characterize physical boundary conditions governing the development of structural deformation features and failure indicators, special emphasis was placed on adequate coverage of relevant areas.

Table 4. Shipboard pore-fluid analytical methods.

Analysis	Method
Salinity	Goldberg refractometer
pH, alkalinity	Automatic titration
Calcium	EGTA titration
Magnesium	EDTA titration (corrected for calcium)
Chloride	Mohr titration
Sulfate	DIONEX ion chromatography
Ammonia	Colorimetry
Phosphate	Colorimetry
Silica	Colorimetry
Potassium	Atomic emission spectrometry
Sodium	Atomic emission spectrometry

Sampling Strategy

To accommodate the general objectives, the sampling program for physical properties was planned to fulfill several requirements:

1. To provide a comprehensive record of recovered core properties. Generally sections were processed through the MST prior to subsampling for whole-round samples. Discrete samples were selected on the average of two per section.
2. To cross-correlate shipboard analyses. Samples were selected in conjunction with sedimentologists and structural geologists to identify features of interest. Analyses of physical properties analyses were made on common or adjacent sample intervals.
3. To calibrate downhole logs. Bulk density, porosity, acoustic velocity, and thermal conductivity from core samples provide downhole property variations for core-log data integration.

Laboratory Measurements

Index Properties

Index properties (water content, bulk density, porosity, grain density, and dry density) were calculated from measurements of wet- and dry-sediment weights and wet-sediment volumes. Checks on these measurements were made with selective measurements of dry-sample volume. Samples of approximately 10 cm³ were taken for the determination of index properties. In addition, whole-core determination of bulk density was measured using the GRAPE on the MST for cores that completely filled the liner.

Sample mass was determined aboard ship to a precision of ±0.01 g using a Scitech electronic balance. The sample mass was counter-balanced by a known mass such that only mass differentials of less than 5 g usually were measured. Volumes were determined using a Quantachrome Penta-Pycnometer, a helium-displacement pycnometer. The Quantachrome pycnometer measures volumes to an approximate precision of ±0.02 cm³. Sample volumes were repeated until two consecutive measurements yielded volumes within 0.02 cm³ of each other. A reference volume was run with each group of samples during the first several hundred tests. The standard was rotated between cells in order to check for systematic error. Preliminary results of this exercise suggest the pycnometer is fairly stable for a given cell inset, or sleeve. However, changing sleeves or insets offset the standard calibration by 0.1 cm³.

The tare beaker calibrations, which are used for discrete index property determinations, were checked for mass and volume during the leg. This recalibration was conducted on the basis of calculation of the densities of the beakers, using the corrected weights and volumes measured during the previous leg. The ODP physical properties database was updated with these corrected values.

Water Content

The determination of water content followed the methods of the American Society for Testing and Materials (ASTM) designation D2216 (ASTM, 1989). As outlined in ASTM D2216, corrections are required for salt when measuring marine samples. All measurements were corrected for salt assuming a pore salinity of 36‰. In addition to the recommended water content calculation, we also determined the ratio of the pore-fluid mass to the dry-sediment mass (% dry mass, as presented in ASTM D2216), and the ratio of pore-fluid mass to total sample mass (% wet mass). The equations for each water content calculation are as follows:

$$W_c (\% \text{ dry mass}) = (M_t - M_d)/(M_d - rM_t) \text{ and} \quad (1)$$

$$W_c (\% \text{ wet mass}) = (M_t - M_d) \times (1 + r)/M_t, \quad (2)$$

where M_t = total mass (saturated), M_d = dry mass, and r = salinity.

Bulk Density

Bulk density (ρ) is the density of the total sample, including the pore fluid (i.e., $\rho = M_t/V_t$, where V_t is the total sample volume). Total mass (M_t) was measured using the electronic balance, and the total volume was measured with the helium pycnometer. In high porosity sediment, bulk density was calculated directly using $\rho = M_t/V_t$. A calculation check was performed on the bulk density results using the specific gravity (G_s). The specific gravity was calculated using the measured bulk density and water content as follows:

$$G_s = \rho/[\rho_w - W_c (\rho - \rho_w)], \quad (3)$$

where ρ_w = density of pore fluid and W_c is the water content reported as a decimal ratio of percent dry mass.

Reference values of specific gravity were directly measured with the pycnometer and balance on selected samples from different lithologies. When the specific gravity calculated from the measured bulk density and water content deviated from these reference values for the measured lithologies or from the measured grain density, the bulk density reported was calculated from water content and grain density. The calculated bulk density values are used in the raw data tables as ρ_{calc} and were determined as follows:

$$\rho_{calc} = ((1 + W_c) / [1 + [W_c \times (\rho_{grain} / \rho_w)]]) \times \rho_{grain}, \quad (4)$$

where W_c is the water content reported as a decimal ratio of percent dry mass.

Porosity

Porosity (ϕ) was calculated using the following equation:

$$\phi = (W_c \times \rho) / [(1 + W_c) \times \rho_w], \quad (5)$$

where ρ used in the equation is either the directly measured bulk density or ρ_{calc} ; W_c is the water content reported as a decimal ratio of percent dry weight.

Grain Density

The grain density (ρ_{grain}) was determined directly on selected intervals from the dry mass (Scitech balance) and dry volume (pycnometer) measurements. Both mass and volume were corrected for salt as follows:

$$\rho_{grain} = (M_d - s) / [V_d - (s/\rho_{salt})], \quad (6)$$

where V_d = dry mass, s = mass of salt in the pore fluid, and ρ_{salt} = density of salt (2.257 Mg/m³).

Dry Density

Dry density (ρ_d) is the ratio of the dry mass (M_d) to the total volume (V_t). The dry density was calculated using the corrected water content and porosity for each measurement:

$$\rho_d = (\phi/W_c) \times \rho_w. \quad (7)$$

Multisensor Track

The Multisensor track (MST) incorporates the gamma-ray attenuation porosity evaluator (GRAPE), P-wave logger (PWL), and magnetic susceptibility sensors in scans of the whole-round core sections. Individual unsplit core sections were placed horizontally on the MST, which moves the section through the three sets of sensors.

The GRAPE makes measurements of bulk density at 1-cm intervals by comparing the attenuation of gamma rays through the cores with attenuation through an aluminum standard (Boyce, 1976). The GRAPE data are most reliable in APC and undisturbed XCB and RCB cores. In disturbed material, the GRAPE was turned off.

The PWL transmits a 500-kHz compressional wave pulse through the core at a repetition rate of 1 kHz. The transmitting and receiving transducers are aligned perpendicular to the core axis. A pair of displacement transducers monitor the separation between the compressional wave transducers; variations in the outside diameter of the liner therefore do not degrade the accuracy of the velocities. Measurements are taken at 2-cm intervals. Generally, only the APC and undisturbed XCB and RCB cores were measured.

Magnetic susceptibility was measured on all sections at 3-cm intervals using the 0.1 range on the Bartington meter with an 8-cm-diameter loop. The close sampling was performed to provide another measure for between-hole correlation. The quality of these results degrades in XCB and RCB sections where the core is undersized and/or disturbed. However, the general downhole trends were used for stratigraphic correlation.

Velocimetry

Compressional wave (*P*-wave) velocity measurements were obtained using two different systems during Leg 146, depending on the degree of lithification of the sediment. The *P*-wave velocities in softer sediments were measured using a Dalhousie University/Bedford Institute of Oceanography digital sound velocimeter (DSV). Velocity calculation is based on the accurate measurement of the time for an acoustic signal to travel between a pair of piezoelectric transducers inserted in the split sediment cores. Two transducers separated by approximately 7 cm were used to measure the vertical (along the core axis) *P*-wave velocity. The transducers are firmly fixed at one end to a steel plate so that their separation does not change during velocity determinations. The transducers emit a 2- μ s square wave at about 250 and 750 kHz. A dedicated microcomputer controls all functions of the velocimeter. The transmitted and received signals are digitized by a Nicolet 320 digital oscilloscope and transferred to the microcomputer for processing. The DSV software selects the first arrival and calculates sediment velocity; the full waveform is stored for later calculation of attenuation. All velocity data reported here are corrected for in-situ temperature and pressure using the following (Wyllie et al., 1956):

$$1/V_{corr} = 1/V_{meas} + \phi/V_{in-situ} - \phi/V_{lab} \quad (8)$$

where V_{corr} = corrected velocity, V_{meas} = measured velocity, $V_{in-situ}$ = the calculated velocity of seawater at in-situ temperature and pressure (using Wilson, 1960), and V_{lab} = the calculated velocity of seawater at the laboratory temperature and pressure (using Wilson, 1960).

Periodically, the separation was evaluated by running a calibration procedure in distilled water. A value of sound velocity in distilled water was determined (based on standard equations) for the measured temperature and the transducer separation was calculated from signal traveltime.

The Hamilton Frame velocimeter was used to measure compressional wave velocities at a signal frequency of 500 kHz in discrete sediment samples for which induration made it difficult to insert the DSV transducers without cracking the sample and in lithified sediments and basement rocks where insertion was impossible. Samples were cut carefully using a double-bladed diamond saw. Sample thickness was measured directly from the velocimeter-frame lead screw through a linear resistor output to a digital multimeter. Delays for the transducers were estimated by linear regression of traveltime vs. distance for a series of aluminum and Lucite standards. Filtered seawater was used to improve the acoustic contact between the sample and the transducers. The DSV oscilloscope and processing software were used

to digitize waveforms, calculate velocities, and store the waveforms. The routine procedure of measurement was to propagate the waveform parallel to the core axis (longitudinal) and across the core, parallel to the split surface (horizontal or transverse). This approach provides a measure of the acoustic anisotropy within the sediments.

Undrained Shear Strength

The undrained shear strength (S_u) of the sediment was determined using the ODP motorized miniature vane shear device following the procedures of Boyce (1976). The vane rotation rate was set to 50°/min. Measurements were made only in the fine-grained units from soft to very stiff consistencies. The vane used for all measurements has a 1:1 blade ratio with a dimension of 1.27 cm.

The instrument measures the torque and strain at the vane shaft using a torque transducer and potentiometer, respectively. Output for torque and strain are recorded on a PC-compatible computer. The shear strength reported is the peak strength determined from the torque vs. strain plot. In addition to the peak shear strength, at selected intervals, the residual strength was determined from the same plot where the failure was not dominated by cracking of the sample (Pyle, 1984).

In the analyses of vane tests the assumption is made that a cylinder of sediment is uniformly sheared about the axis of the vane in an undrained condition, with cohesion as the principal contributor to shear strength. Departures from this assumption include progressive cracking within and outside of the failing specimen, uplift of the failing core cylinder, drainage of local pore pressures (i.e., the test can no longer be considered to be undrained), and stick-slip behavior.

In some sediments, where progressive cracking occurred prior to failure, measurements were made using the pocket penetrometer. The pocket penetrometer is a small, flat-footed cylindrical probe that is pushed into the split core 6.4 mm. The resulting resistance is the unconfined compressive strength or $2S_u$. A scale directly reads out in units of kg/cm². The values of unconfined compression are converted to values of S_u and are reported in units of kPa.

Electrical Resistivity

Two different resistivity devices were used during Leg 146. Both methods utilize a four-probe configuration (Wenner spread) with two current and two potential electrodes. An alternating current is applied to the two outer electrodes and the potential drop across the two inner electrodes is measured. One device, constructed by the University of Bremen, applies a 5-volt alternating square wave across the outer electrodes and measures the potential drop between two platinum electrodes with a 0.2-mm spacing. This device has a built in thermistor to register sediment temperature. The Bremen probe was used to measure resistivity in the soft to stiff sediment. The second device, supplied by the Bedford Institute of Oceanography, applies a 5-volt alternating current to the outer electrodes and measures the potential drop across two gold-plated electrodes, spaced 0.15 mm apart. Because of the smaller probe size, this device was used in very stiff sediment.

Both devices give the resistance of the saturated sediment in terms of the potential drop in mV. In determining sediment resistivity, the potential is first converted to resistance by dividing by the instrument current. The resistance is then converted to resistivity by multiplying by the instrument cell constant. The cell constant is defined as the cross-sectional area divided by the length between the two voltage electrodes. The cell constant was determined for each instrument by measuring the resistance of a known fluid (seawater) at controlled temperatures.

Electrical resistivity of the sediments was measured on all good-quality cores. The electrodes were pushed approximately 2 mm into the split-core surface. For consistency, measurements were made with the probes aligned across the core diameter. These measurements

were used to determine formation factor and to estimate porosity. Formation factor (F) is the ratio of the resistivity of the saturated sediment to the resistivity of the pore fluid. Porosity of the sediment was estimated from formation factor following a modified Archie equation (Lovell, 1984) as follows:

$$F = a \phi^{-m}, \quad (9)$$

where a and m = coefficients that vary with sediment type and ϕ = porosity.

The coefficients for each lithology were determined by plotting F vs. measured porosity and fitting an exponential curve to these data, assuming a constant value for the cementation coefficient (m) of 1.76.

Thermal Conductivity

The thermal conductivity of cored material was measured every 1.0–1.5 m using the needle probe method, in full-space configuration for soft sediments (von Herzen and Maxwell, 1959), and in half-space mode (Vacquier, 1985) for lithified sediment and hard-rock samples. All measurements were made after the cores had equilibrated to the laboratory temperature. Data are reported in units of $W/(m \cdot K)$, and have an estimated error of 5%–10%.

Soft Sediment "Full-space" Measurements

Needle probes containing a heater wire and a calibrated thermistor were inserted into the sediment through small holes drilled in the core liners before the sections were split. The probes were carefully positioned where MST data indicated a sample of uniform properties. Data were acquired using a Thermcon-85 unit interfaced to an IBM-PC compatible microcomputer. This system allowed up to five probes to be connected and operated simultaneously. For quality control, one probe was used with a standard of known conductivity during each run.

At the beginning of each test, temperatures in the samples were monitored without applying a heater current until the background thermal drift was determined to be less than $0.04^\circ C/min$. Once the samples were equilibrated, the heater circuit was closed and the temperature rise in the probes was recorded. Thermal conductivity values were calculated from the rate of temperature rise while the heater current was flowing.

After the heater has been on for about 60 s, the needle probe response is close to that of a line source with constant heat generation per unit length. Temperatures recorded during a time interval of 60–240 s were fitted with the least-squares technique to the appropriate equation:

$$T(t) = (q/4\pi k) \times \ln(t) + L(t), \quad (10)$$

where k = apparent thermal conductivity, T = temperature, t = time, and q = heat input per unit length of wire per unit time.

The term $L(t)$ describes a linear change in temperature with time and includes the background temperature drift and any linearity that results from instrumental errors and the geometrical inadequacies of the experiment. These inadequacies include the finite length of the probe and sample.

All full-space measurements were corrected for a linear offset between measured and true thermal conductivities, determined from a series of tests with standards of known conductivities.

Lithified Sediment and Hard-rock "Half-space" Measurements

Half-space measurements were made on selected samples after the cores had been split, with a needle probe sandwiched between the flat surface of a test sample and that of an epoxy block, which has a

relatively low conductivity (Sass et al., 1984; Vacquier, 1985). All half-space measurements were conducted in a water bath, to keep the samples saturated, to improve the thermal contact between the needle and the sample, and to reduce thermal drift during the tests.

The samples were sanded with 240 and 600 grit paper to smooth the contact area and EE&G thermally conductive compound was used to improve the thermal contact. The data collection and reduction procedures for half-space tests are identical to those for full-space tests.

Probe Calibration

Thermal conductivity probes were calibrated by conducting measurements on three standards of known thermal conductivities. The standards used were red rubber, fused silica, and macor ceramic, all provided by ODP, with known thermal conductivities of, respectively, 0.96, 1.38 and 1.61 $W/(m \cdot K)$. Thermal conductivity readings with the different probes used during Leg 146 are summarized in Table 5. A linear regression of known thermal conductivity, k_{corr} , to probe reading, k_{meas} , indicates a correction given by $k_{corr} = 0.348 + 0.630 k_{meas}$ (Fig. 18). This correction was applied to all readings made during Leg 146.

DOWNHOLE TOOLS

Because primary objectives of Leg 146 included the collection of fluids and characterization of in-situ conditions, a number of special tools were deployed at some of the sites. These tools collectively measure temperature, pressure, lateral stress, pore pressure, permeability, and/or collect interstitial water samples ahead of the drill bit. They include the ADARA APC temperature shoe, the water-sampling temperature probe (WSTP), lateral stress tools (LAST-I and LAST-II), Geoprops probe, and CORK borehole seal. Each of these instruments is described herein, and the data from them are discussed in the site chapters relevant to their respective deployments.

Table 5. Measured and known thermal conductivities of full-space calibration standards.

Standard	Known conductivity [W/(m·K)]	Number of runs	Probe reading mean value [W/(m·K)]	Standard deviation [W/(m·K)]
Red rubber	0.96	52	0.963	0.069
Fused silica	1.38	36	1.665	0.159
Macor ceramic	1.61	32	1.984	0.124

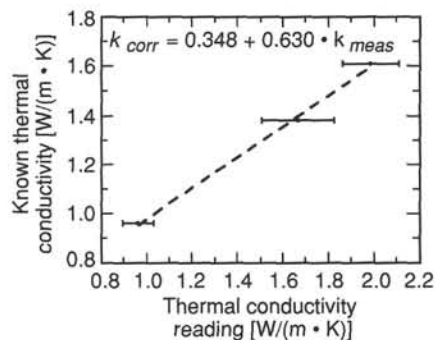


Figure 18. Calibration curve for the three standards used during Leg 146. The standards are red rubber (lowest conductivity), fused silica (middle range conductivity) and macor ceramic (highest conductivity).

Water-sampling Temperature Probe Measurements

The water-sampling temperature probe (WSTP) allows, on a single lowering in a hole, both a pore-water sample and an in-situ temperature measurement to be taken. These functions are effected approximately 1 m ahead of the drill bit, in nominally undisturbed sediment.

The thermistor temperature sensor itself is located inside a narrow, steel cylinder at the base of the pore-water sampling filter (Fig. 19). Probe specifications are given in Table 6.

In operation, the WSTP is lowered down the drill pipe on the sand line while the bit is held above the bottom of the hole. The tool is held briefly above the mud line to equilibrate with the bottom-water temperature, albeit inside the pipe. The tool is then lowered and latched into place, with the temperature-probe tip extending 1.1 m ahead of the bit. The drill string is lowered and the probe is forced into the bottom of the hole. A collet allows the probe to retract back inside the bit should the formation prove to be too hard to penetrate. With an APC/XCB bottom-hole assembly, the bit can be decoupled from the tool after penetration so that the probe will not be disturbed by drill-string heave.

The WSTP has a thermal time constant of several minutes, requiring that the tool remain emplaced for at least 10–15 min in order to allow sufficient equilibration. The theoretical decay curves (Bullard, 1954) used to estimate equilibrium temperature assume instantaneous frictional heating of the probe following penetration. In practice, a finite time is required for the sensors to reach a maximum temperature. As a result, the effective origin time of the thermal pulse is delayed as a function of probe and sediment properties. In addition, the recorder samples temperature at fixed intervals, leaving the exact penetration time uncertain. An effective penetration time and an extrapolated temperature are estimated by shifting the time axis of the theoretical thermal decay curves to fit the actual data. The later parts of the records, >20–50 s following penetration, usually provide a good match. A user-friendly, updated version of the data-processing software was available for its first operational use on Leg 146. It performed satisfactorily in most aspects.

The relatively short length of the narrow temperature probe appears to allow only a few minutes of undisturbed measurement before a thermal disturbance is propagated down from the larger-diameter section above, limiting the accuracy of temperature extrapolations to about $\pm 0.1^{\circ}$ – 0.2° C. Because the exact depth of the tool below the bottom of the hole is never known, all temperatures measured with the WSTP must be considered the lower bounds of in-situ conditions. From the shape of the temperature-time records and comparison with nearby measurements it is often possible to determine if the tool was pressed into fill at the bottom of a hole or if the formation cracked upon insertion. A review of thermal data obtained with early versions of the probe during DSDP is given by Hyndman et al. (1987).

ADARA Temperature Measurements

The ADARA temperature coring shoe, used with the APC, is used to measure in-situ sediment temperature during regular piston-coring operations. The specially designed shoe contains a platinum resistance temperature sensor and the electronic equipment for data acquisition. The latter is built into a cylindrical frame that fits inside an annular cavity in the shoe (Fig. 20). The temperature sensor is located inside one of the two prongs that extend from the base of the frame and anchor the electronics to the shoe. The tool runs on standard camera batteries. Collected data are stored in nonvolatile memory. Data acquisition parameters including the initial and final acquisition times and the data acquisition rate are programmable after the tool has been inserted into the coring shoe. During Leg 146, data were collected at a 5- to 10-s intervals. Other specifications are given in Table 6.

In operation, the shoe is placed on the end of a core barrel and lowered down the pipe. The shoe is usually held above the mud line

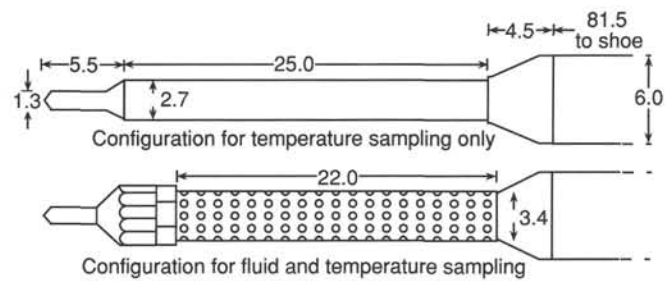


Figure 19. Scale cross-sections of the WSTP probe assembly, configured for temperature only, and for temperature and water sampling. All dimensions are in centimeters. The probe tips extend 1.1 m ahead of the bit when latched in place and fully extended.

Table 6. Specifications of temperature measurement instruments used during Leg 146.

Tool	Thermistor housing (°C)	Sensor resolution	Recording interval
APC tool	Steel annular cylinder, I.D.: 0.0617 m O.D.: 0.0907 m	0.01	Programmable, generally 5 s
WSTP	Steel cylindrical probe, 0.0127-m diameter	0.01	4.369 s

Note: I.D. = inner diameter, and O.D. = outer diameter.



Figure 20. Photograph of the ADARA tool electronics, PC-interface box, connecting cable, batteries, and an APC coring shoe.

for 5–10 min to measure bottom-water temperature (inside the pipe), and is then lowered into the hole. The core barrel is deployed in the standard way, fired out through the bit using hydraulic pressure from the rig pumps, but it is left in place for 10 min instead of being retrieved immediately, so that the tool can begin thermal equilibration with the formation. After the core barrel is returned to the ship, the coring shoe is removed and the temperature data are downloaded to a PC for data reduction.

Data reduction for the APC tool is similar to that for the WSTP probe. The newly developed TFIT program for data analysis was successfully used during Leg 146.

Lateral Stress Tools

LAST-II

LAST-II is a new tool designed for the measurement of in-situ lateral stress, strength, elastic modulus, and pore-pressure response. The measurement element of the tool consists of a radially expanding bladder with two pressure sensors (Fig. 21). One sensor measures expansion pressure and the other measures formation pore pressure. The bladder is expanded with a downhole pressure developer system. This pressure developer expands the bladder using a motor-driven piston. Piston displacement is calibrated with bladder expansion to determine the radial displacement of the bladder.

Lateral stress is determined from the lift-off pressure of the stress-strain curve (Fig. 22). Shear modulus and shear strength are determined directly from the stress-strain curve and pore pressure is measured independently. The tool can be programmed for several loading and unloading cycles. For Leg 146, the tool was configured for one load and one unload cycle for each deployment.

LAST-II is deployed on the ODP collected delivery system. The tool is deployed in the same manner as the WSTP. The tool is pushed into the formation approximately 2.6 m below the bottom of hole. The collected delivery system provides additional compensation for drill-string heave.

The measurement components are controlled by a downhole computer system. This system is connected to a PC-compatible computer by means of a serial interface for programming the tool before each deployment and for downloading the collected data following recovery. The tool is programmed to turn on, run through its preprogrammed cycles, and deflate based on elapsed time.

LAST-I

LAST-I was the first phase of development of lateral stress measurement tools for deep-water deployment. This tool was first used on Leg 131, in the Nankai Trough (Shipboard Scientific Party, 1991). LAST-I is a self-contained measurement device with its own software and data memory. It is similar to the ADARA temperature tool in that all of the instrumentation is built into the wall of a cutting shoe that can be deployed on the APC or XCB sampling tools. The ADARA temperature tool computer system is an updated version of the LAST-I design.

LAST-I is pushed into the seabed formation ahead of the drill bit. After insertion into the formation, the tool is left for approximately 20 min while lateral stress and pore pressure are measured and recorded. The tool measures effective lateral stress using three surface-mounted strain gauges positioned equally around the tool and measures absolute pore pressure using a strain-gauge-type pressure transducer (Fig. 23). The tool uses a reverse cutting shoe to minimize disturbance to sediment around the outer wall of the tool.

The tool is programmed before deployment to turn on and off and to increase/decrease its measurement sampling interval through a serial connection to a PC-compatible computer. After recovery, the data are dumped to the PC and can be immediately plotted as lateral stress and pore pressure vs. time. For Leg 146, the tool served as a backup for LAST-II.

Geoprops Probe

The Geoprops probe is a small straddle packer that carries a data logger to record temperature and pressure, and contains three 20-mL sample bottles (Fig. 24). It is deployed in an open hole created by the motor-driven core barrel (MDCB) ahead of the drill bit. The tool free-falls from the surface and lands at the coring motor with the packer section extended beyond the drill bit in a hole drilled previously with the MDCB. The packer elements and other functions of the Geoprops probe are controlled by drill-pipe pressure. During deployment the rig pumps maintain pressure and circulation in the hole.

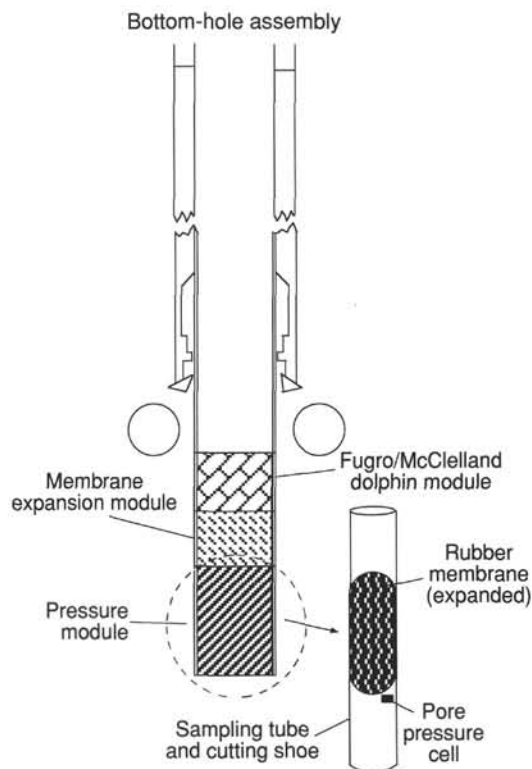


Figure 21. Schematic diagram of the LAST-II showing the three major components: the computer and power supply; the pressure developer; and the pressure meter.

At a preset pressure, the packer elements inflate and press thermistors, pressure-measuring ports, and a fluid-sampling port (all of which are integrated into the packer elements) against the borehole wall. The formation pore pressure and temperature on the face of each packer element are recorded digitally, as well as the pressure between the packers and the annulus pressure. When the packers are pressurized, pore-fluid samples are collected. If the drill-pipe pressure is increased, a volume of water is injected into the interval between the packers, inducing a slug test. The temporal response of the interval pressure yields an in-situ determination of permeability. Upon recovery, the temperature and pressure data are downloaded to a PC.

Leg 146 provided the first field test of the Geoprops probe.

ODP Borehole Seal (CORK)

Two borehole seals (CORKs) were installed on Leg 146, at Sites 889 and 892. These devices, which are described in detail by Davis et al. (1992), are placed in a slightly modified ODP reentry cone that is seated in 16-in. casing washed into the near-surface sediment. An 11 $\frac{3}{4}$ -in. casing is drilled in below this assembly to a depth of 200–300 mbsf and carefully grouted to the formation to prevent leakage to the seafloor. A small-diameter (5.5 in.) casing is hung from the 11 $\frac{3}{4}$ -in. pipe to the bottom of the hole, so that hole collapse will not impair fluid circulation to the sensors. For Leg 146, the small casing was perforated ($\frac{3}{8}$ -in. holes; 9.5% open area) over 50-m sections, at depths appropriate to the suspected aquifers at each site.

Three Nitrile seals near the base of the CORK provide hydraulic isolation of the hole by compression-fit to the 11 $\frac{3}{4}$ -in. casing. The remainder of the CORK, which extends above the reentry cone when seated (Fig. 25), contains a data logging unit and fluid port, so that temperature and pressure are recorded and fluids may be collected from the hole. On Leg 146 deployments, the 16-channel data logger

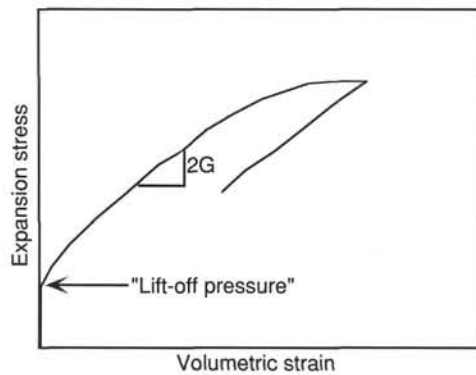


Figure 22. Example test result from an on-land LAST-II field test. The tangent to the stress strain curve is used to determine shear modulus and the initial "lift-off" stress is interpreted as the average lateral stress.

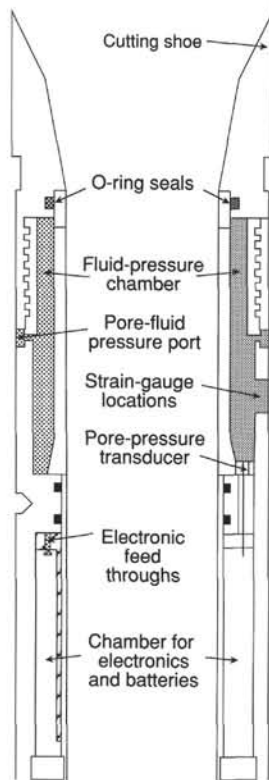


Figure 23. Schematic of the LAST-I tool. The tool is deployed on the APC. Note the reverse cutting shoe, which reduces the disturbance to the outside of the tool.

is connected to 10 thermistors, two tilt sensors, and a pressure transducer. Although the thermistors are positioned over the entire depth of each hole, they are concentrated around the bottom-simulating reflector at Site 889 and the thrust fault zone at Site 892. A $\frac{3}{8}$ -in. (I.D.) Teflon sampling tube is normally bundled with the thermistor string (held taut with an iron sinker bar); however, because of deployment difficulties, this device was not included in the installations at Sites 889 and 892. The fluid line at the base of the data logger was connected to a titanium valve and Teflon sampling port. The data logger is capable of storing data over a 2-yr period, and maintaining that data for another year. Data are downloaded through a 9600-baud RS-232 link. This operation requires use of a submersible or remotely

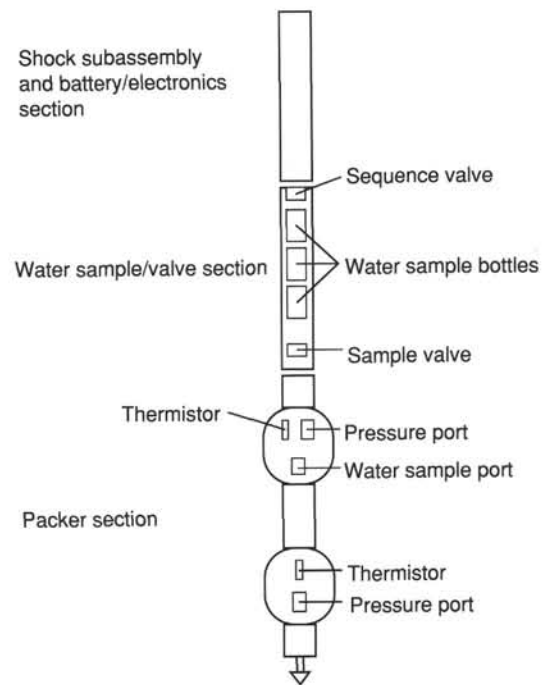


Figure 24. Diagram of Geoprops probe. The upper section contains the data logger, pressure transducers, computer interface, and a shock sub assembly to reduce deceleration of the tool at the bottom of the pipe. The water sample/valve section houses three 20-mL water bottles and valves to control the sequential operation of the tool, water sampling, and the pressure slug injected into the interval between the packer elements. The packer section includes the two inflatable elements which contain temperature, pressure, and (upper element only) water sample ports. The tool is 5.6 m long, 8.9 cm in diameter.

operated vehicle (ROV) to join the underwater-connector and initiate the data dump.

PACKER EXPERIMENTS

Average formation permeability measurements were obtained by means of a resettable drill-string packer manufactured by TAM International and described by Becker (1986, 1988). This packer incorporates inflatable rubber elements to isolate a section of the hole, and can be configured as a single or a straddle packer. For the measurements during Leg 146, it was configured with the two elements used together as a double packer to isolate the zone between the bottom of the hole and the seal (Fig. 26). The packer was inflated in casing near the seafloor and used to measure the average permeability of the entire interval from the base of the cement to the bottom of the hole.

The packer is actuated using a "go-devil" that is dropped down the drill string into the packer inflation subassembly. The go-devil also carries recorders to monitor downhole fluid pressures in the isolated, pressurized zone during the experiment; these pressures are the primary data from which permeability is calculated. Two types of pressure recorders were used during Leg 146: (1) mechanical K-3 gauges made by the Kuster Company and (2) electronic ERPG-300 gauges made by Geophysical Research Corporation. The K-3 gauges record analog pressure mechanically by scratching a metal chart; the ERPG-300 gauges electronically record up to 10,000 digital pressure values, at 8.64-s intervals. The data from either of these gauges are not available until the go-devil is retrieved upon completion of the experiment. However, the entire drill string as well as the isolated zone was pressurized during testing, and a pressure transducer at the rig floor was also used to provide a real-time indication of downhole

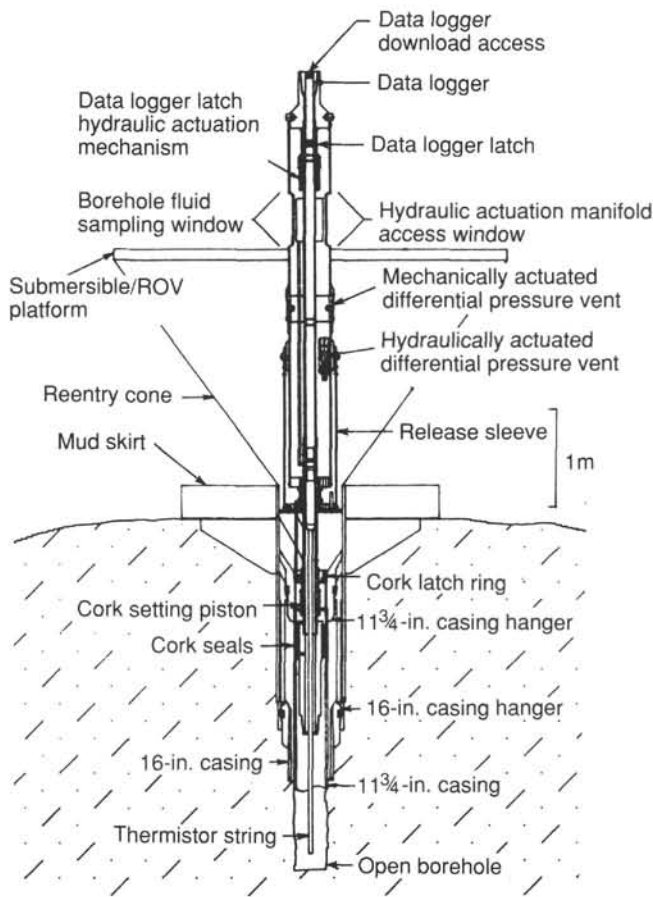


Figure 25. Schematic view of the instrumented borehole seal, including reentry cone and casing, the CORK seal, the data logger, and the thermistor string/sampling tube.

events. Throughout the packer measurements, pumping rates and total volumes pumped were also measured at the rig floor.

Once the packer was inflated, pressure pulse, or "slug," tests were used to determine the permeability of the isolated interval. The methods used were similar to those described by Anderson and Zoback (1982), Hickman et al. (1984), Anderson et al. (1985), and Becker (1989, 1991) in conducting packer experiments in DSDP/ODP Holes 395A and 504B.

Slug Test Procedures

The slug tests were conducted following the methods for the "modified" slug test of Bredehoeft and Papadopoulos (1980), which is an adaptation of the slug test method of Cooper et al. (1967) and Papadopoulos et al. (1973) for formations with relatively low permeability values. In the modified slug test, a short pressure pulse is applied to the fluid in the zone isolated by the packer, and the decay of this pulse is monitored as fluid flows from the borehole into the isolated formation. The decay of such a pressure pulse is described by the equation:

$$P(t)/P_o = F(\alpha, \beta), \quad (11)$$

where P is pressure in excess of the initial undisturbed value, P_o is the initial pressure increase, α is a dimensionless parameter that depends on the storage coefficient (S) and porosity (ϕ) of the isolated formation, β is a dimensionless parameter that depends on the trans-

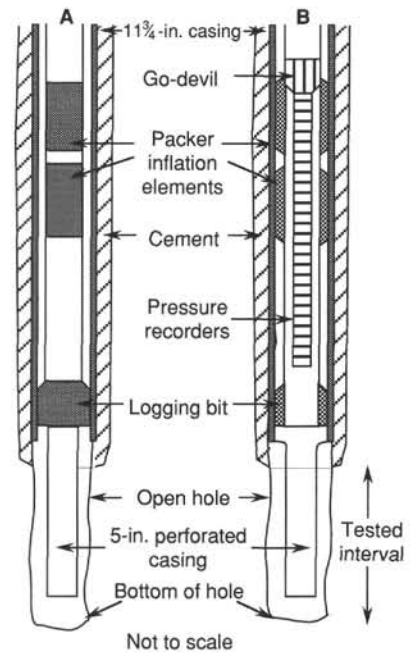


Figure 26. Sketch of the inflatable drill-string packer as deployed during Leg 146. **A.** The double-element packer incorporated in the bottom-hole assembly, before inflation or after deflation. **B.** Cut-away sketch of the inflated packer showing go-devil, pressure recorders, and tested interval between the base of the cement and the bottom of the hole. Note that a 5-in. perforated pipe was installed below the 11 3/4-in. casing but is not cemented. During inflation of the packer, the go-devil directs fluids pumped from the rig floor into the inflation elements; once the packer is inflated, the go-devil position is shifted such that fluids pumped from the rig floor are directed into the tested interval.

missivity (T) and permeability (k) of the formation, and F is a complicated infinite integral. More specifically,

$$\alpha = \pi a^2 S / V_w C_w \rho_w g, \quad (12)$$

$$\beta = \pi T t / V_w C_w \rho_w g, \quad (13)$$

$$S = b \phi C_i \rho_i g, \text{ and} \quad (14)$$

$$T = b k \rho_i g / \mu, \quad (15)$$

where t is time; g is gravitational acceleration; a is the radius of the hole in the isolated zone; b is the height of the isolated zone; C_i , ρ_i , and μ are, respectively, the compressibility, density, and dynamic viscosity of the fluid in the isolated zone; and C_w and ρ_w are the compressibility and density of the fluid in the total pressurized volume V_w .

To process the pressure data measured during slug tests, we followed the standard curve-fitting method described by Cooper et al. (1967) and Papadopoulos et al. (1973), as follows: a plot of the decay of measured pressures as a function of log time was superposed on a family of type-curves of $F(\alpha, \beta)$ as a function of log β calculated for various values of α spanning several orders of magnitude. The data plot was then shifted along the abscissa of the type-curve plot to determine visually the value of α for the type curve which best fit the data. Then the transmissivity and average permeability of the tested interval could be calculated from the correspondence between the values of time and β for the best-fit curve, using Equations 13 and 15. Because the initial undisturbed pressure in the borehole is unknown, the standard curve-matching procedure was modified by varying this parameter to find the best estimate.

As noted by Cooper et al. (1967), Papadopoulos et al. (1973), Bredehoeft and Papadopoulos (1980), and Hickman et al. (1984), this procedure yields relatively poor estimates of the storage coefficient and porosity, but reasonable determinations of transmissivity and average permeability.

Properties of the Fluids in the Pressurized System

The transient pressures measured during both slug and injection tests depend on the properties of the pressurized fluids, particularly viscosity and compressibility, which vary with both temperature and pressure. For the temperature-dependent viscosity of seawater, we used Gartling's (1977) equation, μ_m (in mPa · s) = $16.68T^{-0.8987}$, with T in °C. As noted by Neuzil (1982), the effective compressibility of the fluid in a shut-in hole is sometimes greater than that of the pure fluid (seawater in this case), because of (1) compliance of the drill string and test equipment and (2) air possibly trapped in the system. Although every effort was made during Leg 146 to purge all air from the drill string, pump, and connecting plumbing, small amounts of air may have remained in the system. Such trapped air would increase the effective system compressibility and cause the transmissivity and bulk permeability calculated in a slug test to be erroneously high. Therefore, we carefully recorded the volumes pumped downhole during slug tests, so that the effective compressibility of the pressurized system could be determined using the definition of compressibility, $C = dV/VdP$, and accounted for in the calculation of formation permeability.

Constant-rate Injection Tests

In a constant-rate injection test, borehole pressure within the isolated zone is monitored as fluids are pumped into the formation at a constant rate. The increase in pressure as injection proceeds can be described by:

$$P(a,t) = (q\mu/4\pi kb) \ln(\gamma\phi\mu C_a^2/4kt), \quad (16)$$

where q is the flux of injected fluids, γ is Euler's constant, and the remaining parameters are as previously defined. The transmissivity and average permeability of the isolated zone are determined from the slope of a plot of pressure as a function of the logarithm of time, given the measured constant injection rate. Pressure during shut-in following a constant-rate injection test can be approximated by:

$$P(a,t) = (q\mu/4\pi kb) \ln(t'/t), 128 \quad (17)$$

where t' is time since injection began, and t is time since shut-in. The transmissivity and average permeability of the isolated zone are determined from the slope of a plot of pressure as a function of the natural logarithm of t'/t .

In-situ Permeability vs. Calculated Bulk Permeability

Slug tests involve an important assumption: that the permeability of the rock in the zone isolated by the packer is uniform and isotropic. This assumption is probably not valid for the formations penetrated during Leg 146, where permeability may be dominated by fault-zone or stratigraphic conduits. The permeability values computed here are average Darcian or equivalent porous-medium permeabilities, denoted as bulk permeabilities, obtained by applying the theory for uniformly permeable media. If the in-situ permeability is indeed dominated by isolated fault-zone or stratigraphic conduits, the actual hydrologic conductivity measurements of such conduits may be orders of magnitude greater than the bulk transmissivity values reported here.

DOWNHOLE LOGGING

Logging Tool Strings

Downhole logs can be used to determine directly the physical and chemical properties of formations adjacent to a borehole. Interpretation of these continuous, in-situ measurements can yield a stratigraphic, lithologic, geophysical, and mineralogic characterization of the site. After coring is completed at a hole, a tool string (a combination of several sensors) is lowered downhole on a seven-conductor cable, and each of the sensors in the tool string continuously monitors some property of the adjacent borehole. Although the depths of investigation are sensor-dependent, all data are typically recorded at 15-cm intervals. Four Schlumberger tool strings were used on Leg 146: the geophysical (quad-combo) combination, geochemical combination, Formation MicroScanner, and well seismic tool (WST). During Leg 146, the geophysical string was run at five holes, the FMS was run at four holes, the WST was run at two holes and the geochemical string was run at one hole. The Woods Hole Oceanographic Institution (WHOI) downhole geophone was used at one hole. The Lamont-Doherty Geological Observatory (LDGO) temperature tool was attached to the base of the first- and last-run tool strings at every site, to obtain heat-flow information.

The geophysical tool string used on Leg 146 is a digital string that consists of the long-spaced sonic (LSS), natural gamma-ray tool (NGT), high-temperature lithodensity tool (HLDT), the compensated neutron porosity tool (CNT), and the phasor induction tool (DIT). The geophysical tool string measures compressional wave velocity and provides indicators of the two variables that most often control velocity: porosity, as indicated by density or resistivity, and clay content, as indicated by the NGT. The sonic velocity data, when combined with density data, are used to calculate an impedance log and generate a synthetic seismogram for the logged section. The NGT is run on each tool string to detect depth shifts between tool strings. The HLDT also contains a caliper, which is useful for log quality control. At Hole 892C, the geophysical tool string was divided and run as two strings: the seismic stratigraphic string (LSS, DIT, and NGT) and the litho-porosity string (HLDT, CNT, and NGT).

The geochemical combination used on Leg 146 consists of the NGT, aluminum clay tool (ACT), and gamma spectrometry tool (GST). This tool combination measures the relative concentrations of silicon, calcium, aluminum, iron, sulfur, hydrogen, chlorine, potassium, thorium, and uranium.

The FMS tool string includes not only the FMS but also a general purpose inclinometer tool (GPIT) that spatially orients the FMS resistivity map of the borehole wall. The tool string also contains an NGT to allow depth correlation of the FMS data with other logs.

Logging Tools

A brief description of logging tools run during Leg 146 is given in the following sections. A detailed description of logging tool principles and applications is provided in many texts (e.g., Schlumberger, 1989; Serra, 1984; Timur and Toksöz, 1985).

Electrical Resistivity

The phasor induction tool provides three different measurements of electrical resistivity, each with a different depth of investigation. Two induction devices (deep and medium resistivity) send high-frequency alternating currents through transmitter coils, creating magnetic fields that induce secondary (Foucault) currents in the formation. These ground-loop currents produce new inductive signals, proportional to the conductivity of the formation, which are recorded by the receiving coils. Measured conductivities then are converted to resistivity. A third device, spherically focused resistivity, measures the current necessary to maintain a constant voltage drop across a fixed interval. Vertical

resolution is about 150 cm for the medium device, 200 cm for the deep resistivity device, and about 75 cm for the focused resistivity device.

Water content and salinity are by far the most important factors controlling the electrical resistivity of rocks. To a first order, resistivity responds to the inverse square root of porosity (Archie, 1942). Other factors influencing resistivity include the concentration of hydrous and metallic minerals, vesicularity, and geometry of interconnected pore space.

Sonic Velocity Measurements

The long-spaced sonic (LSS) tool uses two acoustic transmitters and two receivers to measure the time required for sound waves to travel over source-receiver distances of 2.4, 3.0, and 3.6 m. The difference in compressional wave traveltimes over different distances provides a direct measure of the vertical traveltime of sound in the adjacent formation. The raw data are reported as time required for a sound wave to travel vertically through 0.31 m of formation; these traveltimes are then converted to sonic velocities. Only compressional wave velocity is determined during data acquisition, but waveforms are recorded for post-cruise determination of shear-wave velocities and possibly improved compressional wave velocities. The vertical resolution of the tool is 61 cm. Compressional wave velocity is dominantly controlled by porosity and degree of lithification; both decrease in porosity and increase in lithification cause the velocity to increase.

Natural Gamma-ray Tool

The natural gamma-ray tool (NGT) measures the natural radioactivity of the formation. Most gamma rays are emitted by the radioactive isotope K^{40} and by the radioactive elements of the U and Th series. The gamma-ray radiation originating in the formation close to the borehole wall is measured by a scintillation detector mounted inside the tool. Measurements are analyzed by subdividing the entire incident gamma-ray spectrum into five discrete energy windows. The total counts recorded in each window, for a specified depth in the well, are inverted to give the elemental abundances of K, U, and Th. The final outputs are the total gamma ray (SGR), a uranium-free gamma-ray measurement (CGR), and the concentrations of potassium (POTA, weight% or decimal fraction), thorium (THOR, ppm), and uranium (URAN, ppm). The vertical resolution of the log is about 46 cm.

Because radioactive elements tend to be most abundant in clay minerals, the gamma-ray curve is commonly used to estimate the clay or shale content. There are rock matrices, however, for which the radioactivity ranges from moderate to extremely high values as a result of the presence of volcanic ash, potassic feldspar, or other radioactive minerals.

Mechanical Caliper Device

The mechanical caliper device (MCD) provides a measure of borehole diameter. The hole diameter (HD) log is used to detect washouts or constrictions. Borehole diameter significantly affects many of the other logging measurements, and the hole diameter is an important input to log correction routines. This caliper tool is subject to sticking when formation mud gets into its mechanical parts, resulting in bimodal (fully open or nearly fully closed) readings. In contrast, the hole-diameter measurement produced by the high-temperature lithodensity tool is much more reliable. Consequently, on Leg 146 the MCD tool was used primarily to provide centralization and associated improved log quality for the sonic log rather than to measure hole diameter.

Lithodensity Tool

The high-temperature lithodensity tool (HLDT) uses a Ce^{137} gamma-ray source and measures the resulting flux at fixed distances from the source. Under normal operating conditions, attenuation of gamma rays is chiefly caused by Compton scattering (Dewen, 1983).

Formation density is extrapolated from this energy flux by assuming that the atomic weight of most rock-forming elements is approximately twice the atomic number. A photoelectric effect index is also provided. Photoelectric absorption occurs in the energy window below 150 keV and depends on the energy of the incident gamma ray, the atomic cross section, and the nature of the atom. Because this measurement is almost independent of porosity, it can be used directly as an indicator of matrix lithology. The radioactive source and detector array are placed in a tool that is pressed against the borehole wall by a strong spring arm; the position of this spring arm relative to the tool indicates hole diameter. Excessive roughness of the hole will cause some drilling fluid to infiltrate between the detector and the formation. As a consequence, density readings can be artificially low. Approximate corrections can be applied by using caliper data. The vertical resolution is about 38 cm.

Neutron Porosity Tool

A radioactive source mounted on the CNT sonde emits fast (4 MeV) neutrons into the formation, where they are scattered and slowed by collisions with other nuclei. When the neutrons reach a low energy level (0.025 MeV), they are captured and absorbed by atomic nuclei such as hydrogen, chlorine, silicon, and boron. Because neutrons have an atomic mass similar to that of hydrogen, most neutron slowing is caused by collisions with hydrogen, almost exclusively in water molecules. Therefore, a change in the number of neutrons detected at a receiver can be related to porosity. Because water is present both in pores and as bound water (e.g., clay minerals), neutron porosities measured in the presence of hydrous minerals are overestimates of true porosity. The vertical resolution of the tool is theoretically about 0.25 m, but low signal-to-noise ratio degrades this potential resolution. The accuracy of neutron porosities is also adversely affected by variations in hole size.

Gamma Spectrometry Tool

The induced spectral gamma-ray tool (GST) consists of a pulsed source of 14-MeV neutrons and a gamma-ray scintillation detector. A shipboard computer performs spectral analysis of gamma rays generated by the interactions of neutrons emitted by the source with atomic nuclei in the formation (Hertzog, 1979). Characteristic sets of gamma rays from six elements dominate the spectrum, permitting calculation of six elemental yields: calcium, silicon, iron, chlorine, hydrogen, and sulfur. The tool normalizes their sum, so that the yields do not reflect the actual elemental composition. Instead, ratios of these elemental yields are commonly used in interpreting the lithology, porosity, and salinity of the formation fluid. Shore-based processing is used to compute new elemental yields, as well as absolute dry weight fractions of the major oxides.

Aluminum Clay Tool

Aluminum abundance as measured by the aluminum clay tool is determined by neutron-induced late gamma-ray spectrometry using californium as the chemical source. By placing NaI detectors (NGT tools) both above and below the neutron source, contributions from natural gamma-ray activity can be removed. Calibration to elemental weight percent is performed by taking irradiated core samples of known volume and density and measuring their gamma-ray output while placed in a jig attached to the logging tool (generally after logging). The neutron source and its associated detector also provide an uncalibrated neutron porosity log.

Formation MicroScanner

The Formation MicroScanner (FMS) produces high-resolution microresistivity images of the borehole wall that can be used for detailed sedimentological or structural interpretations and for deter-

mining fracture and breakout orientations. The tool consists of 16 electrodes, or buttons, on each of four orthogonal pads that are pressed against the borehole wall. The electrodes are spaced about 2.5 mm apart and are arranged in two diagonally offset rows of eight electrodes each. The focused current that flows from the buttons is recorded as a series of curves that reflect the microresistivity variations of the formation. Shipboard processing converts the measurements into complete, spatially oriented images of the borehole wall. Further processing can provide oriented measurements of strike and dip of planar features. The vertical resolution of the FMS is about 2 cm, but lateral coverage is restricted to about 22% of the borehole wall for each pass of the tool.

Applications of the FMS images include detailed correlation of coring and logging depths, orientation of cores, mapping of fractures, faults, foliations, and formation structures, and the determination of strikes and dips of bedding. The FMS can also be used to measure the orientation of the in-situ stress field, by imaging the directions of borehole breakouts. In an isotropic, linearly elastic rock subjected to an anisotropic stress field, breakouts form in the direction of the least principal horizontal stress. Bell and Gough (1979) and Zoback et al. (1988) demonstrated that the stress orientations deduced from such rock breakouts are consistent with other independent stress indicators. An important limitation of the tool is the restriction of hole diameter to less than 37 cm (14.5 in.); in larger holes, two of the four pads lose contact with the borehole wall and the remaining two pads have lower than optimum pressure on the borehole wall.

General Purpose Inclinator Tool

The GPIT contains a three-component magnetometer, which measures tool orientation with respect to the Earth's magnetic field; from this measurement, borehole inclination is calculated. The tool also determines tool motion from an accelerometer. It is run with the FMS to provide spatial orientation for the borehole wall images.

LDGO Temperature Tool

The LDGO self-contained temperature tool can be attached to any Schlumberger tool string. Data from two thermistors and a pressure transducer are collected at a predetermined rate of one sample per 0.5 to 5.0 s and stored in a Tattletale computer within the tool. Following the logging run, data are dumped from the Tattletale to a shipboard computer for analysis. A fast-response, lower accuracy thermistor is able to detect sudden, very small temperature excursions caused by fluid flow from the formation. A slow-response, higher accuracy thermistor can be used to estimate heat flow, if the history of drilling-fluid circulation in the hole and at least two temperature logs are available (Jaeger, 1961). Data are recorded as a function of time; conversion to depth can be based on the pressure transducer or, preferably, on simultaneous recording by Schlumberger of both depth and time. On Leg 146, we alternated use between two temperature tools; one tool had both fast- and slow-response thermistors, whereas the second contained only a slow-response thermistor.

Vertical Seismic Profiles

Vertical seismic profile (VSP) experiments performed during Leg 146 provide a critical link in the increasing scale of observation (from core measurements, to downhole logs, to seismic reflection data) by tying borehole measurements to the surface seismic data. Heterogeneity in an accretionary prism may mean that the near-borehole region sampled by the sonic log is not representative of that imaged by surface seismic data. The VSP determines interval velocities at seismic frequencies, thereby bridging the gap between the sonic log and surface seismic data. In addition, seismic data are a function of time, whereas borehole measurements are a function of depth; the VSP (which measures traveltime to known depths) establishes the time/

depth relationship necessary to place borehole observations in the regional context provided by conventional seismic data.

Three zero-offset VSPs were successfully obtained on Leg 146 (Holes 889B, 891C, and 892C). Two separate seismic sources, a 400-in.³ water gun and a 300-in.³ air gun, were fired alternately (sequence of shots from one source, followed by sequence of shots from the other). The guns were suspended side by side from buoys attached to a yoke and moored to the aft port crane; horizontal offset was approximately 48.5 m. Gun depths were 4.5 m below sea surface for the water gun and 5.5 m for the air gun; shot time was detected by blast phones suspended 3 m beneath each gun. In addition, a far-field source signature was recorded from a hydrophone suspended approximately 150 m below the sea surface. At Sites 891 and 892, both guns were fired at 2000 psi. At Site 889, both guns were fired at 1300 psi throughout much of the experiment because of firing problems. At Site 889, water-gun stations from 126 to 208 mbsf were taken after obtaining the air-gun data, because of gun problems during the experiment. At all sites, each receiver location recorded at least 6 shots each of air-gun and water-gun data; however, many stations have 30–40 shots with usable first-break data.

The VSPs at Sites 889 and 892 were recorded in open borehole, using the Schlumberger vertical-component well seismic tool (WST). The depth interval between clamping positions was 5 m for most stations, but increased to 8 m in regions of enlarged borehole diameter near the top of Site 889. Data were recorded at a 1-ms sample interval by the Schlumberger Cyber system, and also on a Sun workstation using software developed at the University of Hawaii. Initial shipboard processing was done with Schlumberger Quick-Look software; additional shore-based processing will be done at Hawaii Institute of Geophysics.

At Site 891 the zero-offset VSP was run in open borehole in conjunction with a 2-ship oblique seismic experiment using a three-component geophone provided by Woods Hole Oceanographic Institution (WHOI). A detailed description of the WHOI tool can be found in Shipboard Scientific Party (1990a). Data were recorded at a 2-ms sample interval on the Sun workstation, shore-based processing will be done at Hawaii Institute of Geophysics.

Log Data Quality

The quality of log data may be seriously degraded by excessively large sections of the borehole or by rapid changes in the hole diameter. Resistivity and velocity measurements are less sensitive to borehole effects, whereas the nuclear measurements (density, neutron porosity, and both natural and induced spectral gamma ray) are more sensitive because they are strongly attenuated by the borehole fluid. Corrections can be applied to the original data to reduce the effects of these conditions.

Logs from different tool strings may have small depth mismatches, caused by either cable stretch or ship heave during recording. Small errors in depth matching can impair the multilog analyses in zones of rapidly varying lithology. To minimize the effects of ship heave, a hydraulic heave compensator adjusts for rig motion during logging operations. Precise depth matching of logs with cores is difficult in zones where core recovery is low because of the inherent ambiguity of placing the recovered section within the interval cored.

Log Analysis

During logging, incoming data are observed on a monitor oscilloscope and simultaneously recorded on disk in the Schlumberger logging unit. After logging, data are output to tape, which is read by computer in the downhole measurements laboratory and reformatted to be compatible with the Terralog log-interpretation software package. Most log interpretation (except geochemical log analysis) is carried out aboard ship; further analysis and interpretation are undertaken after the cruise.

Synthetic Seismograms

Synthetic seismograms are generated from an impedance log, which is calculated from the velocity and bulk-density logs. In many cases, a simple constant density is assumed. Experience shows that assuming constant density often gives surprisingly good results, because both velocity and density are usually controlled by the same parameter: porosity. When velocity and density are highly correlated, synthetic seismograms using either a constant density or an actual density log are virtually identical.

The sonic velocity and density logs are input to a program that generates an impedance log (velocity \times density), which is converted from depth to time and then is convolved with a wavelet that is appropriate for the original seismic profile. A 6-Hz wavelet is capable of a vertical resolution on the order of 7-15 m (depending on interval velocity), so reflectors cannot generally be attributed to any small-scale lithologic horizons. The synthetic seismogram, which is calculated using a convolutional model, includes interbed multiples.

ONSHORE PROCESSING OF GEOCHEMICAL LOGGING DATA³

Geochemical Tool String

The geochemical logging tool string (GLT) consists of four separate logging tools: the natural gamma-ray spectrometry tool (NGT), the compensated neutron tool (CNT), the aluminum activation clay tool (AACT), and the gamma-ray spectrometry tool (GST) (all tool abbreviations are trademarks of Schlumberger). A schematic drawing of the GLT, which was run in Hole 891C on Leg 146, is shown in Figure 27. These four tools use three separate modes of gamma-ray spectroscopy for a comprehensive elemental analysis of the formation. The NGT is located at the top of the tool string so that it can measure the naturally occurring radionuclides (thorium, uranium, and potassium) before the formation is irradiated by the nuclear sources contained in the lower tools (Fig. 27). The CNT, located below the NGT, carries a low-energy californium (²⁵²Cf) neutron source to activate the Al atoms in the formation. The AACT, a modified NGT, is located below the ²⁵²Cf source, measuring the activated gamma rays in the formation. By combining the AACT measurement with the previous NGT measurement, the background radiation is subtracted out and a reading of formation Al is obtained (Scott and Smith, 1973). The gamma-ray spectrometry tool, at the base of the string, carries a pulsed neutron generator to induce prompt-capture gamma-ray reactions in the borehole and formation and an NaI(Tl) scintillation detector to measure the energy spectrum of gamma rays generated by the prompt neutron capture reactions. As each of the elements in the formation is characterized by a unique spectral signature, it is possible to derive the contribution (or yield) of each of the major elements silicon, iron, calcium, titanium, sulfur, gadolinium, and potassium from the measured spectrum and, in turn, to estimate the relative abundance of each in the formation when combined with the elemental concentrations from the NGT and AACT. The GST also measures the hydrogen and chlorine in the borehole and formation, although these elements are not used for determining the rock geochemistry.

The only major rock-forming elements not measured by the geochemical tool string are magnesium and sodium; the neutron-capture cross sections of these elements are too small relative to their typical abundances for the GLT to detect. A rough estimate of Mg + Na can be made in some instances by using the photoelectric factor (PEF), measured by the lithodensity tool (Hertzog et al., 1989). This calculation was not implemented on the geochemical data from Hole 891C as

the GST and PEF data in combination were of insufficient quality; the results of the Mg + Na calculation have been found to erroneous in many ODP logging environments (Bristow et al., 1992; Pratson et al., 1993).

Data Reduction

The well-log data from the Schlumberger tools are transmitted digitally up a wireline and are recorded and processed on the *JOIDES Resolution* in the Schlumberger Cyber Service Unit (CSU). The results from the CSU are made available as "field logs" for initial shipboard interpretation. Subsequent reprocessing is necessary to correct the data for the effects of fluids added to the well, logging speed, and drill-pipe interference. Processing of the spectrometry data is required to transform the relative elemental yields into oxide weight fractions.

The processing is performed with a set of log-interpretation programs written by Schlumberger that have been slightly modified to account for the lithologies and hole conditions encountered in ODP holes. The steps are summarized below.

Step 1: Reconstruction of Relative Elemental Yields from Recorded Spectral Data

This first processing step compares the measured spectra from the gamma-ray spectrometry tool with a series of "standard" spectra to determine the relative contribution (or yield) of each element. These "standards" approximate the spectrum of each element. Using a weighted, least-squares inversion method, the relative elemental yields are calculated at each depth level. Six elemental standards (Si, Fe, Ca, S, Cl, and H) are used to produce the shipboard yields, but three additional standards (Ti, Gd, and K) can be included in the post-cruise processing to improve the fit of the spectral standards to the measured spectra (Grau and Schweitzer, 1989). Although Ti, Gd, and K often appear in the formation in very low concentrations, they can make a large contribution to the measured spectra because they have large neutron-capture cross sections. For example, the capture cross section of Gd is 49,000 barns, whereas that of Si is 0.16 barns (Hertzog et al.,

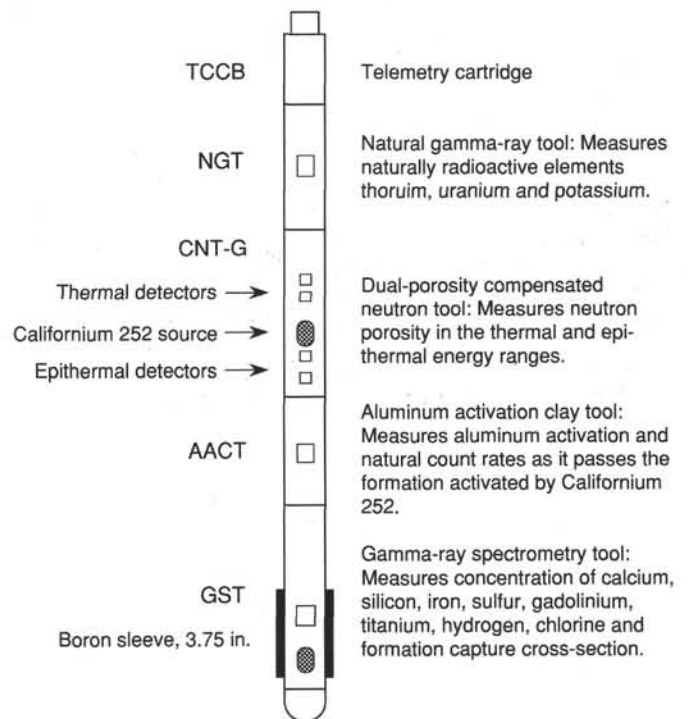


Figure 27. Schematic drawing of the Schlumberger geochemical logging tool string used in the Ocean Drilling Program.

³ Onshore processing of data obtained from the run of the geochemical tool string in Hole 891C was done by J.F. Bristow (Borehole Research, Department of Geology, University of Leicester, Leicester, LE1 7RH, Great Britain) and Cristina Broglia (Borehole Research Group, Lamont-Doherty Earth Observatory of Columbia University, Palisades, NY 10964, U.S.A.).

1989). Therefore, including Gd is necessary when calculating the best fit of the standard spectra to the measured spectrum.

The Si, Ca, Fe, Ti, Gd, K, Cl, and H elemental standards were used in the spectral analysis step for Hole 891C. The spectral standard for S was not used because this element exists in concentrations generally below the detection resolution of the tool in this hole; the inclusion of S in the spectral inversion was found to significantly increase the noise level in the other elemental yields. A linear seven point (3.5 ft, 1.067 m) moving-average smoothing filter was applied to all of the output yields to increase the signal to noise ratio.

Step 2: Depth Shifting

Geochemical processing involves the integration of data from the different tool strings; consequently, it is important that all the data are correlated by depth to one reference logging run. The NGT, run on each of the logging tool strings, provides a spectral gamma-ray curve with which to correlate each of the logging runs. A reference run is chosen on the basis of constant low cable tension and high cable speed (tools run at faster speeds are less likely to stick and are less susceptible to data degradation caused by ship heave). The depth-shifting procedure involves picking a number of reference points based on similar log character and then invoking a program that expands and compresses the matching logging run to fit the reference logging run. The geochemical tool string was chosen as the reference run in Hole 891C.

Step 3: Calculation of Total Radioactivity and Th, U, and K Concentrations

The third processing routine calculates the total natural gamma-ray radiation in the formation, as well as concentrations of Th, U, and K, using the counts in five spectral windows from the NGT (Lock and Hoyer, 1971). This routine resembles shipboard processing; however, the results are improved during post-cruise processing by including corrections for hole-size changes and temperature variations. A Kalman filtering (Ruckebusch, 1983) is used in the CSU processing at sea to minimize the statistical uncertainties in the logs, which can otherwise create erroneous negative values and anti-correlations (especially between Th and U). An alpha filter has been introduced more recently and is now recommended by Schlumberger for shore-based processing. This filter strongly smoothes the raw spectral counts but keeps the total gamma-ray curve unsmoothed before calculating out the Th, U, and K. The outputs of this program are K (wet wt%), U (ppm), and Th (ppm), as well as total gamma-ray and computed gamma-ray (total gamma ray minus U contribution).

Step 4: Calculation of Al Concentration

The fourth processing routine calculates the concentration of Al in the formation using four energy windows recorded on the AACT. During this step, corrections are made for natural radioactivity, borehole-fluid neutron-capture cross section, formation neutron-capture cross section, formation slowing-down length, and borehole size.

Porosity and density logs are needed as inputs into this routine to convert the wet-weight percentages of K and Al curves to dry-weight percentages. Porosity logs from the neutron porosity tool and derived

from resistivity and density logs were compared to core measurements to determine the best core-log correspondence. The neutron porosity log was found to be best in Hole 891C.

A correction is also made for Si interference with Al; the ^{252}Cf source activates the Si, producing the aluminum isotope, ^{28}Al (Hertzog et al., 1989). The program uses the Si yield from the GST to determine the Si background correction. The program outputs dry-weight percentages of Al and K, which are combined in the next processing step with the GST-derived elemental yields in the oxide closure model.

Step 5: Normalization of Elemental Yields from the GST to Calculate the Elemental Weight Fractions

Relative concentrations of the GST-derived elemental yields can be determined by dividing each elemental yield by a relative spectral sensitivity factor (S_i). This factor is principally related to the thermal neutron-capture cross sections and also to its gamma-ray production and detection probability of each element (Hertzog et al., 1989). The relative elemental concentrations are related to the desired absolute concentrations by a depth-dependent normalization factor (F), as defined by the relationship:

$$W_{Ti} = FY_i/S_i \quad (1)$$

where W_{Ti} = absolute elemental concentration, and Y_i = relative elemental yield.

The normalization factor is calculated on the basis that the sum of all the elemental weight fractions is unity (100%). The closure model handles the absence of carbon and oxygen, which are not measured by this tool string, with the approximation that each of the measurable elements combines with a known oxide or carbonate. The dry weight percent of Al and K are normalized with the reconstructed elemental yields to determine the normalization factor at each depth interval from the following equation:

$$F(\sum_i X_i Y_i / S_i) + X_K W_{TK} + X_{Al} W_{TAl} = 100, \quad (2)$$

where X_i = oxide factor, the atomic weight of the associated oxide or carbonate of element i ÷ atomic weight of element i , and where the subscripts K and Al refer to the K and Al components derived from the NGT and AACT, respectively. The value X_i accounts for the C and O associated with each element.

Step 6: Calculation of Oxide Percentages

This routine converts the elemental weight percentages into oxide/carbonate percentages by multiplying each by its associated oxide factor, as shown in Table 7.

Step 7: Calculation of Error Logs

The statistical uncertainty of each element is calculated for each of the elements measured with the GST and NGT (Grau et al., 1990; Schweitzer et al., 1988). This error is strongly related to the normalization factor, which is calculated at each depth level (Eq. 2).

MICROBIOLOGY

Bacteria play a dominant role in the degradation of organic matter within sediments and as a consequence, they drive chemical changes and early diagenesis. Previous research on deep sediment layers (Parkes et al., 1990; Cragg, Harvey, et al., 1992) demonstrated the presence and activity of bacteria to depths in excess of 500 mbsf and their direct involvement in methane cycling within these sediments. The aim of this work is to more accurately quantify rates of bacterial methane production and consumption, the environmental controls on this activity, the organisms involved, and how this is reflected in the $\delta^{13}\text{C}$ of

Table 7. Oxide factors used in normalizing elements to 100% and converting elements to oxides.

Element	Oxide/carbonate	Conversion
Si	SiO ₂	2.139
Ca	CaCO ₃	2.490
Fe	FeO*	1.358
K	K ₂ O	1.205
Ti	TiO ₂	1.668
Al	Al ₂ O ₃	1.889

organic compounds of bacterial origin. This will involve an integrated laboratory analysis (microbial ecology, molecular genetics, organic geochemistry) of whole-round cores stored under sterile and anaerobic conditions, as soon as possible after the collection of samples.

Two types of samples were taken: (1) whole-round cores stored intact for laboratory analysis and (2) 2-cm³ sediment samples preserved for direct determination of bacterial numbers together with porosity and organic matter. Sampling distribution was biased towards the upper 10 m of the holes plus any gas hydrate layers and was coordinated with sampling strategies of organic and inorganic geochemistry.

Whole-round cores were cut from a special 3-m core section comprising two 1.5-m sections left uncut on the catwalk on which the core caps had not been sealed with acetone. The 3-m sections of core were brought into the core reception area, cleaned, wiped with ethanol and placed into a special sterile cutting rig (Cragg et al., 1992) that was constantly flushed with sterile oxygen-free nitrogen (OFN) to maintain anaerobic conditions around the core. One end of the whole-round core was cut with a sterile hacksaw blade, removed from the rig and immediately capped with a sterile core end-cap while flushed with OFN from a sterile gassing jet. The core end-cap was then taped to the liner. The cutting rig was cleaned, alcohol washed, and flamed, and the process was then repeated with the other end of the whole-round core. Cores were sealed within a gas-tight laminated plastic/aluminum bag (Cragg et al., in press) containing a chemical oxygen scrubber (Anaerocult A, Merk) to provide anaerobic conditions. Sealed, anaerobic core sections were held at 4°C before being analyzed.

A 2-cm³ sample was taken from the end of selected 1.5-m sections immediately after cutting on the catwalk and before the sections were sealed with an end-cap. Potentially contaminated sediment was first removed using a sterile scalpel. Then, using a sterile 5-cm³ plastic syringe with the luer end removed, a 2-cm³ minicore sample was taken. The syringe barrel was sealed with a sterile sub-seal stopper. In a clean area of the laboratory, the first 1 cm³ was extruded into a sterile, preweighed, serum vial containing 9 mL of filter-sterilized (0.2 µm), 4% formaldehyde in artificial seawater. The vial was crimped and shaken vigorously to disperse the sediment particles and then stored at 4°C. The remaining 1 cm³ was extruded into a clean, preweighed glass sample vial before porosity determinations and CHN analyses.

REFERENCES*

- Anderson, R.N., and Zoback, M.D., 1982. Permeability, underpressures, and convection in the oceanic crust near the Costa Rica Rift, eastern equatorial Pacific. *J. Geophys. Res.*, 87:2860–2868.
- Anderson, R.N., Zoback, M.D., Hickman, S.H., and Newmark, R.L., 1985. Permeability versus depth in the upper oceanic crust: in situ measurements in DSDP Hole 504B, eastern equatorial Pacific. *J. Geophys. Res.*, 90:3659–3669.
- Archie, G.E., 1942. The electrical resistivity log as an aid in determining some reservoir characteristics. *J. Pet. Tech.*, 5:1–8.
- ASTM, 1989. *Annual Book of ASTM Standards for Soil and Rock; Building Stones: Geotextiles* (Vol. 04.08): Philadelphia (Am. Soc. Testing Materials).
- Banerjee, S.K., and O'Reilly, W., 1967. The behaviour of ferrous ions in iron-titanium spinels. *J. Phys. Chem. Solids*, 28:1323–1335.
- Barnes, R.O., 1988. ODP in situ fluid sampling and measurement: a new wireline tool. In Masche, A., Moore, J.C., et al., *Proc. ODP, Init. Repts.*, 110: College Station, TX (Ocean Drilling Program), 55–63.
- Basov, I.A., Rea, D.K., Janecek, T., et al., in press. *Proc. ODP, Init. Repts.*, 145: College Station, TX (Ocean Drilling Program).
- Becker, K., 1986. Special report: development and use of packers in ODP. *JOIDES J.*, 12:51–57.
- , 1988. A guide to ODP tools for downhole measurements. *ODP Tech. Notes*, 10.
- , 1989. Measurements of the permeability of the sheeted dikes in Hole 504B, ODP Leg 111. In Becker, K., Sakai, H., et al., *Proc. ODP, Sci. Results*, 111: College Station, TX (Ocean Drilling Program), 317–325.
- , 1991. In-situ bulk permeability of oceanic gabbros in Hole 735B. In Von Herzen, R.P., Robinson, P.T., et al., *Proc. ODP, Sci. Results*, 118: College Station, TX (Ocean Drilling Program), 333–348.
- Behrmann, J.H., Lewis, S.D., Musgrave, R.J., et al., 1992. *Proc. ODP, Init. Repts.*, 141: College Station, TX (Ocean Drilling Program).
- Bell, J.S., and Gough, D.I., 1979. Northeast-southwest compressive stress in Alberta: evidence from oil wells. *Earth Planet. Sci. Lett.*, 45:475–482.
- Berggren, W.A., Kent, D.V., and Van Couvering, J.A., 1985. The Neogene: Part 2. Neogene geochronology and chronostratigraphy. In Snelling, N.J. (Ed.), *The Chronology of the Geological Record*. Geol. Soc. London Mem., 10:211–260.
- Biscaye, P.E., 1964. Mineralogy and sedimentation of the deep-sea sediment fine fraction in the Atlantic Ocean. *Geochem. Techn. Rep.*, 8:803.
- Blow, W.H., 1969. Late middle Eocene to Recent planktonic foraminiferal biostratigraphy. In Brönniman, P., and Renz, H.H. (Eds.), *Proc. First Int. Conf. Planktonic Microfossils, Geneva, 1967*: Leiden (E.J. Brill), 1:199–422.
- Boyce, R.E., 1976. Definitions and laboratory techniques of compressional sound velocity parameters and wet-water content, wet-bulk density, and porosity parameters by gravimetric and gamma ray attenuation techniques. In Schlanger, S.O., Jackson, E.D., et al., *Init. Repts. DSDP*, 33: Washington (U.S. Govt. Printing Office), 931–958.
- Bredheoef, J.D., and Papadopoulos, S.S., 1980. A method for determining the hydraulic properties of tight formations. *Water Resour. Res.*, 16:223–238.
- Bristow, J.F., Broglia, C., deMenocal, P.B., and Pratson, E.L., 1992. Data report: geochemical logging results from the Sea of Japan: Sites 798 and 799. In Tamaki, K., Suyehiro, K., Allan, J., McWilliams, M., et al., *Proc. ODP, Sci. Results*, 127/128 (Pt. 2): College Station, TX (Ocean Drilling Program), 1395–1410.
- Bullard, E.C., 1954. The flow of heat through the floor of the Atlantic Ocean. *Proc. R. Soc. London A*, 222:408–429.
- Cande, S.C., and Kent, D.V., 1992. A new geomagnetic polarity time scale for the Late Cretaceous and Cenozoic. *J. Geophys. Res.*, 97:13917–13951.
- Cooper, H.H., Jr., Bredheoef, J.D., and Papadopoulos, I.S., 1967. Response of a finite diameter well to an instantaneous charge of water. *Water Resour. Res.*, 3:267–269.
- Cragg, B.A., Bale, S.J., and Parkes, R.J., in press. A novel method for the transport and storage of bacterial samples under anaerobic conditions. *Letts. Appl. Microbiol.*
- Cragg, B.A., Harvey, S.M., Fry, J.C., Herbert, R.A., and Parkes, R.J., 1992. Bacterial biomass and activity in the deep sediment layers of the Japan sea, Hole 798B. In Pisciotto, K.A., Ingle, J.C., Jr., von Breymann, M.T., Barron, J., et al., *Proc. ODP, Sci. Results*, 127/128 (Pt. 1): College Station, TX (Ocean Drilling Program), 761–776.
- Davis, E.E., Becker, K., Pettigrew, T., Carson, B., and MacDonald, R., 1992. Cork: a hydrologic seal and downhole observatory for deep-ocean boreholes. In Davis, E.E., Mottl, M.J., Fisher, A.T., et al., *Proc. ODP, Init. Repts.*, 139: College Station, TX (Ocean Drilling Program), 43–53.
- Dewan, J.T., 1983. *Essentials of Modern Open-Hole Log Interpretation*: Tulsa (PennWell).
- Espitalié, J., 1980. Role of mineral matrix in kerogen pyrolysis: influence on petroleum generation and migration. *AAPG Bull.*, 64:59–66.
- Espitalié, J., Deroo, G., and Marquis, F., 1985a. La pyrolyse Rock-Eval et ses applications. *Rev. Inst. Fr. Pet.*, 40/5:563–579.
- , 1985b. La pyrolyse Rock-Eval et ses applications. *Rev. Inst. Fr. Pet.*, 40/6:755–784.
- , 1986. La pyrolyse Rock-Eval et ses applications. *Rev. Inst. Fr. Pet.*, 41:73–89.
- Fisher, R.V., and Schmincke, H.-U., 1984. *Pyroclastic Rocks*: New York (Springer-Verlag).
- Foreman, H.P., 1975. Radiolaria from the North Pacific, Deep Sea Drilling Project, Leg 32. In Larson, R.L., Moberly, R., et al., *Init. Repts. DSDP*, 32: Washington (U.S. Govt. Printing Office), 579–676.
- Gartling, D.K., 1977. Convective heat transfer analysis by the finite element method. *Comput. Methods Appl. Mech. Eng.*, 12:365–382.
- Gieskes, J.M., Gamo, T., and Brumsack, H.J., 1991. Chemical methods for interstitial water analysis aboard *JOIDES Resolution*. *ODP Tech. Note*, 15.
- Grau, J.A., and Schweitzer, J.S., 1989. Elemental concentrations from thermal neutron capture gamma-ray spectra in geological formations. *Nucl. Geophys.*, 3:1–9.

* Abbreviations for names of organizations and publication titles in ODP reference lists follow the style given in *Chemical Abstracts Service Source Index* (published by American Chemical Society).

- Grau, J.A., Schweitzer, J.S., and Hertzog, R.C., 1990. Statistical uncertainties of elemental concentrations extracted from neutron-induced gamma-ray measurements. *IEEE Trans. Nuclear Sci.*, 37:2175–2178.
- Hays, J.D., 1970. Stratigraphy and evolutionary trends of radiolaria in North Pacific deep sea sediments. In Hays, J.D. (Ed.), *Geological Investigations of the North Pacific*. Mem.—Geol. Soc. Am., 126:185–218.
- Hays, J.D., and Shackleton, N.J., 1976. Globally synchronous extinction of radiolarian *Stylactractus universus*. *Geology*, 4:649–652.
- Hertzog, R., 1979. Laboratory and field evaluation of an inelastic-neutron-scattering and capture gamma-ray spectroscopy tool. *Soc. Pet. Eng. Pap.*, 7430.
- Hertzog, R., Colson, L., Seeman, B., O'Brien, M., Scott, H., McKeon, D., Wraight, J., Grau, J., Ellis, D., Schweitzer, J., and Herron, M., 1989. Geochemical logging with spectrometry tools. *SPE Formation Evaluation*, 4:153–162.
- Hickman, S.H., Langseth, M.G., and Svitek, J.F., 1984. In situ permeability and pore-pressure measurements near the mid-Atlantic Ridge, Deep Sea Drilling Project Hole 395A. In Hyndman, R.D., Salisbury, M.H., et al., *Init. Repts. DSDP*, 78 (Pt. 2): Washington (U.S. Govt. Printing Office), 699–708.
- Hyndman, R.D., Langseth, M.G., and Von Herzen, R.P., 1987. Deep Sea Drilling Project geothermal measurements: a review. *Rev. Geophys.*, 25:1563–1582.
- Ihmle, P.F., Hirt, A.M., Lowrie, W., and Dietrich, D., 1989. Inverse magnetic fabric in deformed limestones of the Morcles Nappe, Switzerland. *Geophys. Res. Lett.*, 16:1383–1386.
- Ingle, J.C., 1980. Cenozoic paleobathymetry and depositional history of selected sequences within the Southern California continental borderland. *Spec. Publ. Cushman Found. Foraminiferal Res.*, 19:163–195.
- Ishikawa, Y., 1967. Magnetic properties of a single crystal of Fe_2TiO_4 . *Phys. Lett. A*, 24:725–727.
- Jaeger, J.C., 1961. The effect of the drilling fluid on temperatures measured in boreholes. *J. Geophys. Res.*, 66:563–569.
- Johnson, D.A., Schneider, D.A., Nigrini, C.A., Caulet, J.P., and Kent, D.V., 1989. Pliocene-Pleistocene radiolarian events and magnetostratigraphic calibrations for the tropical Indian Ocean. *Mar. Micropaleontol.*, 14:33–66.
- Katz, B.J., 1983. Limitations of "Rock-Eval" pyrolysis for typing organic matter. *Org. Geochem.*, 4:195–199.
- Kelts, K., Curry, J.R., and Moore, D.G., 1982. Introduction and explanatory notes. In Curry, J.R., Moore, D.G., et al., *Init. Repts. DSDP*, 64 (Pt. 1): Washington (U.S. Govt. Printing Office), 5–26.
- Kligfield, R., and Channell, J.E.T., 1981. Widespread remagnetization of Helvetic Limestones. *J. Geophys. Res.*, 86:1888–1900.
- Kling, S.A., 1973. Radiolaria from the eastern North Pacific, Deep Sea Drilling Project Leg 18. In Kulm, L.D., von Huene, R., et al., *Init. Repts. DSDP*, 18: Washington (U.S. Govt. Printing Office), 617–671.
- Lagoe, M.B., and Thompson, P.R., 1988. Chronostratigraphic significance of Late Cenozoic planktonic foraminifera from the Ventura Basin, California: potential for improving tectonic and depositional interpretation. *J. Foraminiferal Res.*, 18:250–266.
- Lock, G.A., and Hoyer, W.A., 1971. Natural gamma-ray spectral logging. *The Log Analyst*, 12:3–9.
- Lovlie, M.A., 1984. Thermal conductivity and permeability assessment by electrical resistivity measurements in marine sediments. *Mar. Geotechnol.*, 6:205–240.
- Lowrie, W., 1990. Identification of ferromagnetic minerals in a rock by coercivity and unblocking temperature properties. *Geophys. Res. Lett.*, 17:159–162.
- Lundberg, N., and Moore, J.C., 1986. Macroscopic structural features in Deep Sea Drilling Project cores from forearc regions. In Moore, J.C. (Ed.), *Structural Fabrics Preserved in Deep Sea Drilling Project Cores from Forearcs*. Mem.—Geol. Soc. Am., 166:13–44.
- Manheim, F.T., and Sayles, F.L., 1974. Composition and origin of interstitial waters of marine sediments based on deep sea drill cores. In Goldberg, E.D. (Ed.), *The Sea* (Vol. 5): New York (Wiley Interscience), 527–568.
- Matthews, D.J., 1939. *Tables of Velocity of Sound in Pore Water and in Seawater*: London (Admiralty, Hydrogr. Dept.).
- Mazzullo, J.M., Meyer, A., and Kidd, R., 1987. New sediment classification scheme for the Ocean Drilling Program. In Mazzullo, J., and Graham, A.G. (Eds.), *Handbook for Shipboard Sedimentologists*. ODP Tech. Note, 8:45–67.
- Morley, J.J., 1985. Radiolarians from the Northwest Pacific, Deep Sea Drilling Project Leg 86. In Heath, G.R., Burckle, L.H., et al., *Init. Repts. DSDP*, 86: Washington (U. S. Govt. Printing Office), 399–422.
- Morley, J.J., Hays, J.D., and Robertson, J.H., 1982. Stratigraphic framework for the late Pleistocene in the northwest Pacific ocean. *Deep-Sea Res. Part A*, 29:1485–1499.
- Munsell Soil Color Charts, 1971. Baltimore, MD (Munsell Color).
- Musgrave, R.J., Delaney, M.L., Stax, R., and Tarduno, J.A., 1993. Magnetic diagenesis, organic input, interstitial water chemistry, and paleomagnetic record of the carbonate sequence on the Ontong Java Plateau. In Berger, W.H., Kroenke, L.W., Mayer, L.A., et al., *Proc. ODP, Sci. Results*, 130: College Station, TX (Ocean Drilling Program), 527–546.
- Neuzil, C.E., 1982. On conducting the modified "slug" test in tight formations. *Water Resour. Res.*, 18:439–441.
- Papadopoulos, S.S., Bredehoeft, J.D., and Cooper, H.H., 1973. On the analysis of "slug test" data. *Water Resour. Res.*, 9:1087–1089.
- Parkes, R.J., Cragg, B.A., Fry, J.C., Herbert, R.A., and Wimpenny, J.W.T., 1990. Bacterial biomass and activity in deep sediment layers from the Peru margin. *Philos. Trans. R. Soc. London A*, 331:139–153.
- Peters, K.E., 1986. Guidelines for evaluating petroleum source rock using programmed pyrolysis. *AAPG Bull.*, 70:318–329.
- Pratson, E.L., Broglia, C., and Jarrard, R., 1993. Data report: geochemical well logs through Cenozoic and Quaternary sediments from Sites 815, 817, 820, 822, and 823. In McKenzie, J.A., Davies, P.J., Palmer-Julson, A., et al., *Proc. ODP, Sci. Results*, 133: College Station, TX (Ocean Drilling Program), 795–817.
- Pyle, M.R., 1984. Vane shear data on undrained residual strength. *J. Geotech. Engr. Div., Am. Soc. Civ. Eng.*, 110:543–547.
- Riedel, W.R., and Sanfilippo, A., 1970. Radiolaria, Leg 4, Deep Sea Drilling Project. In Bader, R.G., Gerard, R.D., et al., *Init. Repts. DSDP*, 4: Washington (U.S. Govt. Printing Office), 503–575.
- , 1971. Cenozoic radiolaria from the western tropical Pacific, Leg 7. In Winterer, E.L., Riedel, W.R., et al., *Init. Repts. DSDP*, 7 (Pt. 2): Washington (U.S. Govt. Printing Office), 1529–1672.
- , 1978. Stratigraphy and evolution of tropical Cenozoic radiolarians. *Micropaleontology*, 24:61–96.
- Ruckebusch, G., 1983. A Kalman filtering approach to natural gamma ray spectroscopy in well logging. *Inst. Electr. Electron. Eng. [trans., on autom. contr.]*, AC-28(3):372–380.
- Sanfilippo, A., Westberg-Smith, M.J., and Riedel, W.R., 1985. Cenozoic radiolaria. In Bolli, H.M., Saunders, J.B., and Perch-Nielsen, K. (Eds.), *Plankton Stratigraphy*: Cambridge (Cambridge Univ. Press), 631–712.
- Sass, J.H., Kennelly, J.P., Jr., Smith, E.P., and Wendt, W.E., 1984. Laboratory line-source methods for the measurement of thermal conductivity of rocks near room temperature. *U.S. Geol. Surv. Tech. Rep.*
- Schlumberger, 1989. *Log Interpretation Principles/Applications*: Houston, TX (Schlumberger Educational Services).
- Schweitzer, J.S., Grau, J.A., and Hertzog, R.C., 1988. Precision and accuracy of short-lived activation measurements for in situ geological analyses. *J. Trace Microprobe Techniques*, 6:437–451.
- Scott, H.D., and Smith, M.P., 1973. The aluminum activation log. *Log Anal.*, 14:3–12.
- Serra, O., 1984. *Fundamentals of Well Log Interpretation* (Vol. 1): *The Acquisition of Logging Data*: Amsterdam (Elsevier).
- Shepard, F., 1954. Nomenclature based on sand-silt-clay ratios. *J. Sediment. Petrol.*, 24:151–158.
- Shipboard Scientific Party, 1990a. Explanatory Notes. In Gradstein, F.M., Ludden, J.N., et al., *Proc. ODP, Init. Repts.*, 123: College Station, TX (Ocean Drilling Program), 237.
- , 1990b. Explanatory notes. In Rangin, C., Silver, E.A., von Breyman, M.T., et al., *Proc. ODP, Init. Repts.*, 124: College Station, TX (Ocean Drilling Program), 7–33.
- , 1991. Special tools. In Taira, A., Hill, I., Firth, J.V., et al., *Proc. ODP, Init. Repts.*, 131: College Station, TX (Ocean Drilling Program), 61–70.
- Spencer-Cervato, C., Lazarus, D.B., Beckman, J.-P., Perch-Nielsen, K., and Bolli, M., in press. New calibrations of Neogene radiolarian events in the North Pacific. *Mar. Micropaleontol.*
- Taira, A., Hill, I., Firth, J.V., et al., 1991. *Proc. ODP, Init. Repts.*, 131: College Station, TX (Ocean Drilling Program).
- Timur, A., and Toksöz, M.N., 1985. Fundamentals of well log interpretation. *Ann. Rev. Earth Planet. Sci.*, 13:315–344.
- Vacquier, V., 1985. The measurement of thermal conductivity of solids with a transient linear heat source on the plane surface of a poorly conducting body. *Earth Planet. Sci. Lett.*, 74:275–279.
- Von Herzen, R.P., and Maxwell, A.E., 1959. The measurement of thermal conductivity of deep-sea sediments by a needle-probe method. *J. Geophys. Res.*, 64:1557–1563.

SHIPBOARD SCIENTIFIC PARTY

- Wentworth, C.K., 1922. A scale of grade and class terms of clastic sediments. *J. Geol.*, 30:377-392.
- Wilson, W.D., 1960. Speed of sound in seawater as a function of temperature, pressure and salinity. *J. Acoust. Soc. Am.*, 32:641-644.
- Wyllie, M.R.J., Gregory, A.R., and Gardner, L.W., 1956. Elastic wave velocities in heterogeneous and porous media. *Geophysics*, 21:41-70.
- Wyman, R.E., and Castaño, J.R., 1974. Show descriptions from core, sidewall and ditch samples. *SPWLA 15th Annu. Logging Symp.*, 1-21.
- Zoback, M.D., Zoback, M.L., Mount, V.S., Suppe, J., Eaton, J.P., Healy, J.H., Oppenheimer, D., Reasenber, P., Jones, L., Raleigh, C.B., Wong, I.G., Scotti, O., and Wentworth, C., 1988. New evidence on the state of stress of the San Andreas Fault. *Science*, 238:1105-1111.

Ms 146IR-005